Single Image Signal-to-Noise Ratio Estimation for Magnetic Resonance Images

Mohammadali Kiani Sheikhabadi

Submitted to the
Institute of Graduate Studies and Research
in partial fulfillment of the requirements for the degree of

Master of Science
in
Electrical and Electronic Engineering

Eastern Mediterranean University
July 2015
Gazimağusa, North Cyprus

Approval of the Institute of Graduate Studies and Research

Prof. Dr. Serhan Çiftçioğlu
Acting Director

I certify that this thesis satisfies the requirements as a thesis for the degree of Master of Science in Electrical and Electronic Engineering.

Prof. Dr. Hasan Demirel
Chair, Department of Electrical and
Electronic Engineering

We certify that we have read this thesis and that in our opinion it is fully adequate in scope and quality as a thesis for the degree of Master of Science in Electrical and Electronic Engineering.

Prof. Dr. Sim Kok Swee
Co-Supervisor

Prof. Dr. Hasan Demirel
Supervisor

Examining Committee

1. Prof. Dr. Hasan Demirel
2. Prof. Dr. Hüseyin Özkaramanli
3. Asst. Prof. Dr. Rasime Uyguroğlu

ABSTRACT

Signal-to-noise ratio (SNR) is a significant factor to quantify noise content, particularly in magnetic resonance imaging (MRI). MRI is used to generate high quality medical images in biomedicine and other research areas.

In this thesis, two new approaches of SNR calculation for MRI system is developed and implemented for error minimization. The supreme proposed method applies the cubic spline interpolation with Savitzky-Golay (CSISG) technique in addition to using Gaussian mixture model decomposition (GMMD) algorithm to eliminate the energy of noise and increase the accuracy in SNR estimation. This approach is found to accomplish stunning results while compared with other existing methods as well as cross correlation function (CCF) and cubic spline interpolation with Savitzky-Golay (CSISG) approaches. Unlike other, the suggested approach is based on a single MR image, which generates consistency and accuracy in SNR estimation. A new noise reduction approach, based on cubic spline interpolation with Savitzky-Golay (CSISG) and GMMD, is developed. The GMMD-CSISG represented the tremendous outcome for SNR evaluation of MR imaging systems.

Another technique has been designed to estimate the SNR for MR images. This technique exposed that cross-correlation of two acquisition of the same image could be applied in an extremely efficient approach for the MR system. We conduct several tests on various MRI according to the important characteristics of an MR image such as, phase relative to the RF transmitter phase, frequency, and magnitude. For approximation of perfect noise level shifting a general expression has been originated through a third degree polynomial curve fitting according to outcomes of these experimentations. The

procedure uses single MR image to attain SNR value. The capability to define the SNR from a single MR image allows suggested method to be valid for online and offline image evaluation instantaneously.

Keywords: Signal-to-Noise Ratio, Magnetic Resonance Imaging, Gaussian Mixture Model Decomposition, Auto-Correlation Function, Cross-Correlation Function.

ÖZ

Sinyal-gürültü oranı (SNR), özellikle bir manyetik rezonans görüntüleme (MRI) işleminde, gürültü içeriği ölçmek için önemli bir faktördür. MR biyomedikal ve diğer araştırma alanlarında yüksek kaliteli tıbbi görüntüler oluşturmak için kullanılmaktadır.

Bu tezde, MR sistemi için SNR hesaplama yöntemi olarak iki yeni yaklaşım geliştirilmiştir. Hesaplanan SNR değerlerinin hata minimizasyonu için kullanılması muhtemeldir. Önerilen yöntem Savitzky-Golay (CSISG) gürültü enerjisini ortadan kaldırmak ve SNR tahmininin doğruluğunu artırmak için Gauss karışım modeli ayrışma (GMMD) algoritması kullanılmıştır. Buna ek olarak kübik spline aradeğerleme tekniği uygulanmıştır. Bu yaklaşım diğer mevcut yöntemlerden Savitzky-Golay (CSISG) ve (CCF) kübik spline aradeğerleme yöntemleriyle kıyaslandıgı zaman daha başarılı sonuçlar alınmıştır. Önerilen yaklaşım SNR kestiriminde tutarlılık ve doğruluk üreten tek MR görüntüsüne dayanmaktadır. Savitzky-Golay (CSISG) ve GMMD ile kübik spline aradeğerlendirmeye dayalı yeni bir SNR kestirim yaklaşımı geliştirilmiştir. GMMD-CSISG MR görüntüleme sistemleri SNR hasaplama kestirimi için etkileyici sonuçlar ortaya çıkarmıştır.

MR görüntülerinde SNR tahmin etmek için ikinci bir teknik de önerilmiştir. Bu teknik, aynı görüntünün iki farklı örneğinin çapraz-bağıntısının MR sisteminde SNR hesaplaması için son derece verimli bir yaklaşım olduğunu ortaya çıkarmıştır. Bu tezde birçok MR performans testlerini MR görüntüsünde faz, frekans ve büyüklük gibi önemli özelliklere dayanarak gerçekleştirdik. Mükemmel gürültü seviyasi kaydırılma kestirimi için üçüncü dereceden bir polinom eğrisi ile modellenmiş bir eğri kullanılarak elde edilmiş olan matematiksel bir ifade kullanılmıştır. Prosedür SNR değerini elde etmek için tek MR görüntüsünü kullanmaktadır. Önerilen yöntem çerçevesinde tek bir

MR imgesi kullanarak SNR hesabı yapılabilmesi, gerçek zamanlı ve çevrim dışı görüntü değerlendirme için geçerli alabilecek yaklaşımlar önermemizi mümkün kılabilecek düzeydedir.

Anahtar Kelimeler: Sinyal-Gürültü Oranı, Manyetik Rezonans Görüntüleme, Gauss Karışım Model Ayrışımı, Otomatik Korelasyon Fonksiyonu, Çapraz Korelasyon Fonksiyonu.

To my Family

ACKNOWLEDGMENT

At the outset, I would like to express gratitude to my supervisor Prof. Hasan Demirel for his patience, words of encouragement and invaluable suggestions. Very special thanks to my co-supervisor Prof. Sim Kok Swee for his invaluable guidance, assistance, efficient support, and the great contribution he did throughout this research. I would like to also thank Secretary of Electrical and Electronic department, Ms. Yeliz Evginel for her invaluable contributions during this research.

Besides, I would like to express my appreciation to all members of my family, especially to my father Khodamorad Kiani and my mother Giti Sajjadi, for their continuous support and teaching me how to be myself and follow my dreams in life.

TABLE OF CONTENTS

LIST OF TABLES

LIST OF FIGURES

LIST OF SYMBOLS/ABBREVIATIONS

$\bar{r}(0)$	Noise-Free Autocorrelation Peak
$r(0)$	Noisy Autocorrelation Peak
μ^2	Image Mean
P	Spin Angular Momentum
h	Plank's Constant
I	Nuclear Spin Quantum Number
μ_m	Magnetic Moment
γ	Gyromagnetic Ratio
$r_{11}(x,y)$	Auto-Correlation Function
$P(f)$	Power Spectrum
τ	Averaging Time Interval
$r_{12}(x,y)$	Cross-Correlation Function
$m[i,j]$	Magnitude Signal
φ	Phase Signal Impact
μ_i	Mean
σ_i^2	Variance
$f_i(x)$	Density Function
θ	Unknown Component Parameter
π_i	Mixing Proportion
W_i	Weighting Factor
ε	Best-Fit Equation
$\rho(\vec{i})$	Cross-Correlation Coefficient Centre
SNR	Signal-to-Noise Ratio
MRI	Magnetic Resonance Imaging

INCCE	Image Noise Cross-Correlation Estimation
NV	Noise Variance
AR	Autoregressive
EM	Expectation-Maximization
GMMD	Gaussian Mixture Modeling Decomposition
SEM	Scanning Electron Microscopy
CSISG	Cubic Spline Interpolation with Savitzky-Golay
SIM	Single Image
TIM	Two Images
CCF	Cross-Correlation Function
ACF	Auto-Correlation Function
CCC	Cross-Correlation Coefficient
MLTDEAR	Mixed Lagrange Time Delay Estimation Autoregressive
SNR_{amp}	Amplitude SNR
SNR_{power}	Power of SNR
NMRI	Nuclear Magnetic Resonance imaging
MRT	Magnetic Resonance Tomography
CT	Computed Tomography
PET	Position Emission Tomography
SPECT	Single-Photon Computed Tomography
RF	Radio Frequency
PSD	Power Spectral Density
WSS	Wide-Sense Stationary
FID	Free Induction Decay

Chapter 1

INTRODUCTION

1.1 Introduction

Signal-to-noise ratio (SNR) is a significant element to quantify noise content, particularly in magnetic resonance imaging (MRI). MRI is used to generate high quality medical images in biomedicine and other research areas [1]. Several acquisitions of radiological image techniques such as MR images [2,3], single photon emission calculated tomography [4,5], and positron emission tomography [6] endures from image deterioration by noise. White thermal noise is the primary source for MR images that process an actuarial autonomous random source to enter the MR data in the time domain. The random field including Gaussian probability density function with constant variance and zero mean is depicted by white thermal noise [7,8]. Consequently, the signal is not correlated with noise. The reconstructed MRI characterized by Rice distribution, because of transformation of Fourier Transform [1]. The Rice distribution shape characteristics depend on the SNR; for high SNR, the distribution approaches a Gaussian shape; where at low SNR, the distribution leans to a Rayleigh distribution [9].

A common approach to evaluate the quantity of noise is to calculate the standard deviation of the resultant image [10]. In addition, Murphy et al. [11] developed this approach and utilized a parallel rod analysis object for SNR evaluation. A simple approach to calculate the SNR is to calculate directly non-signal regions or from the noise of a large uniform signal [12]. Both methods approximate the SNR from magnitude MRI, while the noise is Rayleigh distributed; these estimations should be

accomplished with remarkable caution [13]. Another suggested method indicates, which a Cross-correlation method can be applied to evaluate band limited stochastic functions SNR quantities [14].

Afterwards, single image SNR estimation was proposed using image noise cross-correlation estimation (INCCE) technique [15]. The INCCE approach was also utilized for noise variance (NV) estimation in MR images [16].

Gaussian mixture modeling decomposition is one of the most challenging topics in the history of statistic. Gaussian mixture is considered as one of the mixture densities classes. Due to brief and simple illustration of demanding mean μ and the variance σ^2, Gaussian mixture density is known as one of the widespread approaches. The Gaussian density is isotropic, unimodal, symmetric and concerns the least prior knowledge in order to calculate an unknown probability density via a given mean and variance [17]-[18]. Gaussian mixture density based on maximum likelihood prediction technique for non-Gaussian source Autoregressive (AR) parameters, diminishes the error prediction for high SNR [17]. The Expectation-Maximization (EM) is a standard approach to estimate maximum likelihood in Gaussian Finite Mixture models [19]. Nevertheless, almost all of the above-mentioned methods are not precise or robust sufficient for approximating the SNR of MRI. This thesis presents a new developed procedure based on Gaussian mixture model decomposition to reduce the error for SNR evaluation. The idea is to identify the relation between Gaussian mixture model of MR images and their mixing proportions to estimate the ultimate SNR based on our previous work [20]. We estimate the SNR using GMMD based on [18]-[19], where every Gaussian mixture contains the spectra of comparable properties. The results of GMMD-CSISG approach

produce the remarkable SNR estimation for different level of noise 3%, 9%, 15% and 21%.

1.2 Problem Definition

There had been number of work to enhance methods on estimating signal and noise variance (NV) from autocorrelation function (ACF) [21]. In this thesis, As indicated in Fig. 3.1, $\bar{r}(0)$ denoted as power of signal around the zero-offset ACF value of signal curvature and $r(0)$ as power of noise around the zero-offset ACF value of additive noise, where μ is the image mean value, hence, $\bar{r}(0)-\mu^2$ demonstrates the energy of image signal and $r(0)-\bar{r}(0)$ specifies the energy of noisy image [22].

Therefore, the energy of image noise and image signal is developed throughout the autocorrelation function curvature as it is presented in Eq. (1.1) [22]:

$$SNR=\frac{\bar{r}(0)-\mu^2}{r(0)-\bar{r}(0)} \tag{1.1}$$

1.3 Thesis Objectives

Despite the fact that numbers of technique have been developed for SNR estimation of MR imaging systems, nevertheless, though the achievements of these methods are significant, they are not precise or robust enough and extremely reliant on the nature of images.

The motivation to initialization of this project is due to the importance of signal-to-noise ratio (SNR) measurement in image and signal processing especially when it comes to SEM and MR imaging systems and most of approaches are insignificant in accuracy and estimation.

The main focus of this thesis is to provide a precise technique for single image SNR estimation, MR and SEM images are selected for test and outcomes are compared with other existing methods.

1.4 Thesis Contributions

In this thesis two different techniques for estimation of SNR based Gaussian mixture model and Cross-Correlation technique are proposed to provide SNR measurement enhancement.

- The first technique is based on Gaussian Mixture Modeling Decomposition (GMMD) and cubic spline interpolation with Savitzky-Golay (CSISG), which is developed to estimate signal-to-noise ratio (SNR) of magnetic resonance images (MRI), we used both GMMD and CSISG method to generate an robust signal-to-noise ratio estimation.
- In the second technique, Cross-Correlation is used to develop an approach in order to estimate signal-to-noise ratio of magnetic resonance images (MRI) based on mean and standard deviation of single image (SIM).

1.5 Thesis Outline

This thesis includes six chapters. A brief outline to SNR and both GMMD and Cross-correlation are given in Chapter 1. Chapter 2 is a literature review, which discusses the essential models of SNR measurement and estimation, basic mechanisms of MR imaging, as well as advantages and disadvantages of MR images. In chapter 3, a brief explanation on the basic concept of problem formation and reviews existing methods with their performances is given to help the reader to comprehend the basis on which the project was initiated. Chapter 4 explains the proposed solutions and discusses each method in details; the details on enhancement and flow of the project are illuminated step by step. In chapter 5, experimental results of SNR estimation of the proposed and the other existing methods are discussed. The results are discussed and compared. In

chapter 6, the conclusions on the experimental outcomes and the related future work are demonstrated.

Chapter 2

LITERATURE REVIEW

2.1 INTRODUCTION

This chapter introduces the basic concept of signal-to-noise ratio in image processing and theory involved in magnetic resonance imaging and the scanning electron microscope and discusses related works and topics relevant to the research based on the various publications and journals as a reference to this thesis. This chapter highlights the basic imaging techniques involved in the MR images SNR measurement and estimation. This chapter will also discuss the concept of auto-correlation function (ACF), power spectrum, cross-correlation function (CCF) and the Gaussian mixture modeling decomposition (GMMD), which is mainly involved in the proposed SNR estimation method.

2.2 Noise variance estimation

Let *f* be an image obtained as $N \times N$ square tiling, and let *w* be considered white noise source independent of *f*. Then noisy image *g* is obtained by corrupting image *f* with white noise *w* [23].

To estimate noise variance, noise and signal are divided at the output of this edge detector. Around 80 percent in the edge detector amplitude histogram responses was considered as Noise Corporation and used in measurement [24]. But this method is not accurate and even surface fitting and edge detection are not accurate procedures any longer.

Accurate blind noise variance can be obtained while algorithm is implemented on the parallel structure of an image pyramid, thus it might be successful when used on a serial machine [23].

2.3 Signal-to-noise ratio estimation

There is an ordinary way to calculate the noise of an image by computing the standard deviation of the resulting image and calculating difference of two acquisitions of the same object [11]. Another way for SNR estimation is to calculate SNR directly from the non-signal regions or from noise of large uniform signal [12]. The CCF of two images of the similar area is another suggested method in order in order to obtain SNR value [25]. Afterwards, another method proposed is to estimate SNR by a single image [26]. In 2004, a novel technique was proposed to resolve the problems of SNR and the method is according to statistical autoregressive (AR) model to estimate noise free image [27]. A modified method of AR based on several images corruption with various noise level at different elaboration was proposed and called mixed Lagrange time delay estimation autoregressive (MLTDEAR) [28].

2.3.1 Amplitude SNR

In many cases, the SNR is expressed as the ratio of signal amplitude to noise amplitude as it is shown in Eq. (2.1):

$$SNR_{amp} = \frac{Amplitude(S)}{Ampliude(N)} \tag{2.1}$$

Where S is denoted as signal and N is the corrupted noise and SNR_{amp} is called the amplitude SNR. In fact, exact definition of the amplitude SNR depends on the specifying what is meant by “signal amplitude” and “noise amplitude”. Thus, it should particularly be adapted to the specific case it is used for [6].

2.3.2 Power SNR

SNR can be expresses as the ratio of signal power to noise power as it is illustrated in Eq. (2.2):

$$SNR_{power} = \frac{Power(S)}{Power(N)} \tag{2.2}$$

Where SNR_{power} is named the power of SNR, identical as the amplitude SNR the exact description of the power SNR depends on what is meant by "signal power " and "noise power".

2.4 Basic Physics of MR Signals and Imaging

The nuclear magnetic resonance (NMR or MR) phenomenon in majority matter was initially established by Bloch and associates [6] and Purcell and associates [6] in 1946, since when MR has been used in different area with applications in physics, chemistry, biology, and medicine. MRI is a tomographic imaging method, which generates chemical features of an object and images of internal physical from externally estimated MR signals [6].

Magnetic resonance tomography (MRT) or Nuclear magnetic resonance imaging (NMRI) is used as a medical imaging approach in radiology in order to picture the specified inside substances. Since it delivers good contrast among soft tissues of body it has been generally practical especially in muscles, heart and brain while compared with other medical imaging methods such as X-rays or computed tomography (CT). Like any other tomographic imaging technique, the output of MRI scanner is a multidimensional data array (or image), which represents the spatial distributions of some estimated physical quantity. Then MRI may also produce two-dimensional sectional images at any orientation, three-dimensional volumetric images, or even four-dimensional images demonstrating spatial-temporal or spatial-spectral distributions. As a matter of fact no

mechanical modulates to the imaging equipment are required in producing such images. Object itself constructed the image directly using MR signals. In this regard, MRI could be considered as a form of emission tomography similar to single-photon computed tomography (SPECT) and position emission tomography (PET). But unlike the SPECT or PET, no insertion of radioactive isotopes into the object is required for generating of signal in MRI [3]. MR images are tremendously rich in information content and operate in the radio frequency (RF) range. The basic of NMR lies in a property governed by certain nuclei, named the spin angular momentum *p*. The spin angular momentum of the nucleus is a result of the spinning motion or rotational of the nucleus along its own axis. The spin angular momentum of a nucleus is described by the nuclear spin quantum number *I*, and it is illustrated in Eq. (2.3):

$$|P| = \hbar \times \sqrt{\mathrm{I}(\mathrm{I}+1)} \tag{2.3}$$

Where $\hbar = h / 2\pi$ and h is the Planck's constant.

Spin angular momentum is accompanied through a magnetic moment μ_m, while the nucleus is a charged particle**,** as can be seen in Eq. (2.4):

$$\mu_m = \gamma p \tag{2.4}$$

Where γ signified as gyromagnetic ratio.

2.4.1 Nuclei in a Magnetic Field

The performance of nuclei located in an outside magnetic filed is the main concern in MR experiments. The existence of a magnetic moment measures the nucleus behaves as a microscopic bar magnet, then it will connect with a magnetic field. Water includes of two hydrogen nuclei or proton, the body contains large amount of water molecules. The magnetic filed of the scanner causes that the magnetic moments of these protons along with the orientation of the field [29].

In the existence of radio frequency magnetic field the protons adjust their magnetization position relative to the field. At the absence of this filed the protons return to the actual magnetization position. These fluctuations produce a signal that may be perceived via the scanner. There are protons variation in resonance frequency based on the magnetic field strength. The image of the body can be visualized by injecting additional magnetic field throughout the scanning position of the protons [29].

Unwell tissue such as growths can be discovered, as the protons in dissimilar tissues return to their stability at diverse rates. Using this effect and changing the scanner's parameters technically produce contrast among different forms of body substance [29].

2.5 Auto-Correlation Function

The correlation function and its PSD, the Fourier transform, are significantly utilized in identification and modeling of pattern ad structures in image and signal processing. Correlations play a significant role in image processing. The auto-correlation function of an image $f(i,j)$ denoted by $r_{11}(x,y)$, is defined as Eq. (2.5):

$$r_{11}(x,y) = \frac{1}{(2M+1)} \times \frac{1}{(2N+1)} \sum_{i=-M}^{M} \sum_{j=-N}^{N} f(i,j) f(i+x, j+y) \tag{2.5}$$

The auto-correlation function is $r_{11}(x,y)$ an amount of the similarity [1]; it can be used to obtain the repeating patterns such as periodic signal, which has been buried under noise.

2.6 Power Spectral Density

The power spectrum or the power spectral density (PSD) function, of a process presents the distribution spectrum of power at different frequencies [1]. It can be signified that the Fourier transform of the ACF is the power spectrum of a wide-sense stationary (WSS) procedure:

$$P(f) = \sum_{r=-\infty}^{\infty} r_{11}(\tau) e^{-j2\pi f \tau} \tag{2.6}$$

Where τ is the averaging time interval.

2.7 Cross-Correlation Function

In image processing cross-correlation is a measure of similarity of two images. The cross-correlation is basically similar to the convolution of two functions [1]. It is defined in Eq. (2.7):

$$r_{12}(x,y) = \frac{1}{(2M+1)} \times \frac{1}{(2N+1)} \sum_{i=-M}^{M} \sum_{j=-N}^{N} f(i,j) g(i+x, j+y) \tag{2.7}$$

Where $f(i,j)$ and $g(i,j)$ are two images.

2.8 Noise Model for Magnetic Resonance Imaging

The image strength in MR magnitude images in presence of noise is controlled by Rice distribution with constant noise power at each voxel, which produces real and imaginary parts of a corrupted signal with zero-mean uncorrelated Gaussian noise [30]-[31]. This type of noise may be encountered in MR images, speckle and many others [30]. MRI are transformed to magnitude images by estimating the absolute value pixel by pixel from the real and imaginary parts of images [30], as it is displayed in Eq. (2.8):

$$\left| m[i,j] \right| = \sqrt{\left[(s[i,j]\cos(\varphi) + n_{\mathrm{Re}}[i,j])^2 + (s[i,j]\sin(\varphi) + n_{\mathrm{Im}}[i,j])^2 \right]} \tag{2.8}$$

In Eq. (2.8), $m[i,j]$ is the magnitude signal in pixel $[i,j]$, $s[i,j]$ is a signal, n is the noise and φ is the phase signal impact to the imaginary (Im) and real (Re) part in the specific pixel $[i,j]$.

2.9 Gaussian Mixture Modeling

2.9.1 Gaussian Mixture Model Decomposition

In this section Gaussian Mixture Model Decomposition (GMMD) algorithm has been applied in order to estimate the unknown probability densities. Probability density

approximation by classifying a decomposition using GMMD algorithm is successfully applied to the several Magnetic Resonance Images (MRI) for different noise variance level [18].

Gaussian distribution with mean μ_i and variance σ_i^2 derived as Eq. (2.9)

$$f(x;\mu_i,\sigma_i^2) = \frac{1}{\sqrt{2\pi\sigma_i^2}} \exp\left[-\frac{1}{2}\left(\frac{x-\mu_i}{\sigma_i}\right)^2\right] \tag{2.9}$$

Then, for N peaks, the GMMD is obtained by Eq. (2.10):

$$F(x;\mu_i,\sigma_i^2,\theta) = \sum_{i=1}^{N} \pi_i f(x;\mu_i,\sigma_i^2) \tag{2.10}$$

Where θ are the unknown component parameter, which compelled by $0 < \pi_i < 1$ and $\sum_{i=1}^{k} \pi_i = 1$.

2.9.2 Fitting Gaussian Mixture Model To Grouped Data

A Gaussian mixture grouped data can be obtained using maximum likelihood via the EM algorithm [32]. In this section, a k-component finite mixture for the density function is estimated through Eq. (2.11)

$$g(x) = \sum_{i=1}^{k} \pi_i f_i(x) \tag{2.11}$$

Where π_i and $f_i(x)$ are the mixing proportion and component density functions, respectively. Moreover, the unknown parameters regarding of component density functions denoted as θ_i, which in case the case of three-component Gaussian mixture, the parameter vector is $\theta_i = (\mu_i, \sigma_i)$, while $i = 1,2,3$.

2.10 T1 and T2 Weighted Contrast

MR images scanning can differentiate among body substances according to their physical features. MRI scanning is consequently exceptionally valuable at delivering highly detailed images of soft tissues [33]. At MR images scan certain tissues seem to be darker or brighter than other tissues. T1 and T2 Relaxation times for protons can fluctuate and two times are normally evaluated. Darkness depends on the density of protons in that region. White substance is brighter than grey substance in T2-weighted MR sample images and darker than grey substance in T1-weighted MR sample images [33].

Chapter 3

FORMATION OF PROBLEM

3.1 Introduction

This chapter emphasizes the problem in image SNR evaluations that originated the development of this project. A solution to this problem is proposed in the next chapter.

Biomedicine introduces the magnetic resonance imaging as a powerful imaging system, which generates high quality medical images. MRI is also a power full electron microscope that is extensively utilized in metallurgy, biomedicine and biomedical research parts. These images are generally analyzed and processed through advanced digital-data-processing tools, and also contain physiological, anatomical and functional information.

3.2 Image Quality and Noise in MRI

The quality of the MR data highly depends on the available signal-to-noise ratio of the system. With the use of the higher field strength magnets and advances in RF receiving coil design currently MRI scanners have higher SNR than the prototype machines of the late 1970s [6]. However, due to the demand of high spatial resolution and to avoid poor image quality the highest possible SNR is still required [6]. SNR is a useful measure of image quality. SNR is associated to the measurements of signal and the noise or the graininess of a picture. High degree of noise destroys the details of the image. Usually the noise comes from the electronics of the system and is thus unalterable.

SNR in a significant factor in MRI as it can measure the content of noise in an image [6]. MRI, positron emission tomography [6], single photon emission computed tomography [26]-[28] and many radiological image techniques suffer from image corruption by noise. The initial source of noise for MRI is thermal noise. Thermal noise could be considered as white noise and can be illustrated by a Gaussian PDF with constant variance and zero mean [10]-[11]. The noise is not correlated with the signal. Due to Fourier transform noise transformation in MR images could be considered with the Rice distribution. Whereas for low SNR the shape of it leans to a Rayleigh distribution, at high SNR it approaches a Gaussian shape [12]. Noise usually reduces the quality of the image.

MRI contains a set of complex values data that are degraded by Johnson noise [6]. Gaussian PDF is a well model for this set of complex data. Typically, only the scanner delivers the complex data magnitude. In the image the Gaussian noise in complex space is nonlinearly transformed and the subsequent noise is Rician-distributed [6]. At the high SNR, the Rician-distribution can be estimated through a Gaussian distribution [6].

3.3 SNR in MRI

SNR is a main consideration in MRI for numerous reasons. In fact SNR is a measure of image quality; SNR could be utilized to show the implementation of the MR system. The quantification of the SNR is a helpful way to analyze the field homogeneity, the RF amplifiers consistency, and the identity of the radio frequency pulses. The quantity of noise in an image could be estimated thru subtracting two acquisitions of the equivalent entity and the standard deviation of the resultant image [1]. Murphy *et al*. [14] utilized a parallel rod test object for SNR evaluations. Robbie proposed the use of a standard phantom with relaxation times and a loading annulus of known electrical conductivity and geometry for SNR measurements [34].

3.4 Problem Statement

It is surprising that there is not a generally accepted technique for SNR measurement. Parameter estimation is the major problem in the most of MR and SEM image data analysis. For instance, in the case of noise filtering the true signal component is corrupted by noise and an estimation of it is needed. With respect to the importance of SNR in image analysis especially in MR and SEM imaging an accurate method to estimate the SNR for MR and SEM Imaging systems is needed.

3.5 Problem Verification

There had been number of work to enhance methods on estimating signal and noise variance (NV) from autocorrelation function (ACF) [21]. In this paper, As indicated in Fig. 1, $\bar{r}(0)$ denoted as power of signal around the zero-offset ACF value of signal curvature and $r(0)$ as power of noise around the zero-offset ACF value of additive noise, where μ is the image mean value, hence, $\bar{r}(0)-\mu^2$ demonstrates the energy of image signal and $r(0)-\bar{r}(0)$ specifies the energy of noisy image [22].

Therefore, the energy of image noise and image signal is developed throughout the autocorrelation function curvature as it is presented in Eq. (3.1) [22]:

$$SNR = \frac{\bar{r}(0)-\mu^2}{r(0)-\bar{r}(0)} \tag{3.1}$$

As indicated in the Fig. 3.1, Gaussian noise is used to degrade ACF of signal curvature. In this section, $\bar{r}(0)$ is estimated for each Gaussian mixture component of noisy images by eliminating the noise power through CSISG filtering method.

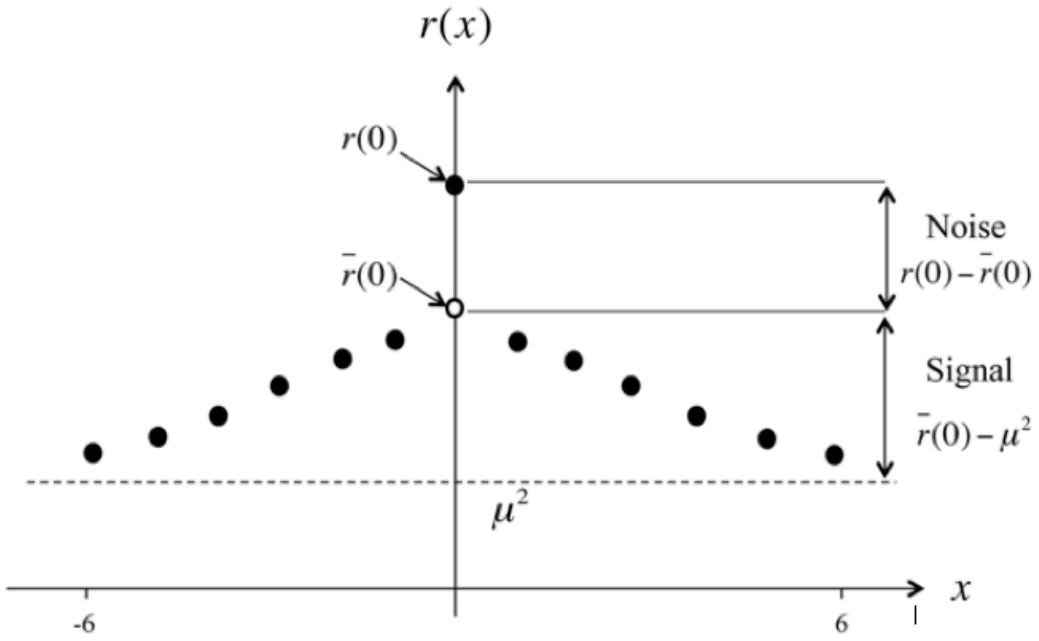

Figure 3.1: ACF of sample image corrupted with white noise [20].

SNR of the MRI can be measured through approximating the noise-free peak of the auto-correlation function curve, using a single image SNR method. The capability to precisely compute the SNR of the MR image depends very much on the correctness of the estimation technique.

In the next chapter, we suggest to use a new approach so that the noise-free peak approximation of the ACF curve and the SNR of the image (i.e. MR and SEM images) can be better quantified, for the benefits of noise reduction.

3.6 Review of Existing SNR Estimators

3.6.1 Cubic spline interpolation with Savitzky-Golay smoothing

Piecewise cubic splines come with first and second order derivatives. Cubic spline interpolation is utilized as an esteemed technique to interpolate between known data points. The cubic spline is originated from function values in nodes and derivative values on the edges of interpolation interval [35].

It is expected that there are a group of identified points $(x_0,r(x_0)),(x_1,r(x_1)),...,(x_{j-1},r(x_{j-1})),(x_j,r(x_j)),(x_{j+1},r(x_{j+1})),...(x_n,r(x_n))$. For every single data point, third order degree polynomial is utilized to interpolate between all the known data points. The equation to the left of point $(x_j,r_j(x_j))$ is achieved as r_{j-1} with a value of $r_{j-1}(x_j)$ at point x_j. Similarly, the equation at the right point of $(x_j,r(x_j))$ is found as r_{j+1} with a value of $r_{j+1}(x_j)$ at point x_j [36].

In the case of polynomial function with the order of three, the curvature will be as $r_j(x)=a_4+a_3x+a_2x^2+a_1x^3$ while the curvature passes within all the known points and $r_j(x_j)$ of the coefficients of curvature function can be estimated [36]. Thus, they all can be accomplished as Eq. (3.2):

$$r_j(x)=\sum_{j=1}^{n+1}a_jx^{n+1-i} \tag{3.2}$$

In the Eq. (3.2), x is signified as ACF of noisy image. Therefore, Coefficients estimation of x based on third order of polynomial can produce the entire curve. However, the Savitzky-Golay smoothing is expended to smooth the constructed curvature $r_j(x)$ by eliminating the noise power in the following section.

3.6.1.1 Savitzky-Golay Smoothing

Based on least square by appropriate fitting a small set of consecutive data point into a polynomial, The SNR of MR or SEM images can be better quantified thru smoothing function. The calculated central of the fitted point polynomial curve is measured as a new smoothed data set [37].

The selected Span level is a percentile of total number of data points, which is less than or equal to 1. These digits can be generated as specifically equivalent for fitting the

data to a polynomial in order to diminish the error in SNR approximation. Savitzky-Golay smoothing demonstrations that the set of digits $(W_{-n}, W_{-(n-1)}, ..., W_{(n-1)}, W_n)$ may be described as weighting coefficients but according to the polynomial degree and desired Span level to implement the smoothing procedure. [37]. Consequently, the smoothed data point is presented in Eq. (5):

$$\bar{r}_j(n) = \frac{\sum_{i=-n}^{n} W_i r_{j+i}}{\sum_{i=-n}^{n} W_i} \tag{3.3}$$

In the Eq. (3.3), $r_j(x)$ signifies a set of smoothed data points with third order of polynomial that is created by cubic spline interpolation, and W_i is the weighting factor in smoothing the window that is produced by desired Span level to create the best-fit line through the line of estimated data (cubic spline interpolation generated data points), it is based on diminishing the error among the estimated and actual ACF of images [20].

As can be realized in Eq. (3.4), ε will be produced to diminish the sum of the squares of the differences ($r(x)$-distances) [38].

$$\varepsilon = \sum (r_j - R_j)^2 \tag{3.4}$$

Formulation of the line is stated to construct the best-fit data R_j for x, while q is slope and c is the r (x)-intercept [38].

$$R_j = qx_j + c \tag{3.5}$$

If we replace Eq. (3.5) into Eq. (3.4), we can obtain a new ex*p*ression for ε (Eq. (3.6)).

$$\varepsilon = \sum (r_j - qx_j - c)^2 \tag{3.6}$$

In order to create the best-fit equation, ε contains of factors (q_{best}, c_{best}) is produced. We utilized partial derivatives in order to minimize ε with respect to only one variable concurrently (*q or c*) [38].

$$\frac{\partial \varepsilon}{\partial q} = \frac{\partial f(q,c)}{\partial q} = 0 \tag{3.7}$$

$$\frac{\partial \varepsilon}{\partial c} = \frac{\partial f(q,c)}{\partial c} = 0 \tag{3.8}$$

We differentiate Eq. (3.7) and (3.8), in order to gain Eq. (3.11), multipliers, which do not vary can be factored out of the summation.

$$\frac{\partial \varepsilon}{\partial q} = 2\sum (r_j - qx_j - c)(-x_j) = 0 \tag{3.9}$$

$$\frac{\partial \varepsilon}{\partial q} = \sum x_j r_j - qx_j^2 - cx_j = 0 \tag{3.10}$$

$$\sum x_j r_j - q_{best} \sum x_j^2 - c_{best} \sum x_j = 0 \tag{3.11}$$

Subsequently, we differentiate Eq. (3.8). Again, Eq. (3.14) has illustrated the same as the earlier step; multiplication by the total number of points is equal to the summation of 1 [38].

$$\frac{\partial \varepsilon}{\partial c} = 2\sum (r_j - qx_j - c)(-1) = 0 \tag{3.12}$$

$$\frac{\partial \varepsilon}{\partial c} = \sum r_j - q\sum x_j - c\sum (1) = 0 \tag{3.13}$$

$$\sum r_j - q_{best} \sum x_j - nc_{best} = 0 \tag{3.14}$$

Eq. (3.11) and (3.14) demonstrate normal equations, the normal equations support to obtain q_{best} and c_{best} [38].

We solve Eq. (3.14) for *c* (Eq. (3.15)) and substitute it into Eq. (3.11) to give Eq. (3.16). Solving for *q* gives Eq. (3.17).

$$c = \frac{q\sum x_j - \sum r_j}{n} \tag{3.15}$$

$$\sum x_j r_j - q\sum x_j^2 - \left[\frac{q\sum x_j - \sum r_j}{n}\right]\sum x_j = 0 \tag{3.16}$$

$$q = \frac{n\sum x_j r_j + \sum x_j \sum r_j}{n\left[\sum x_j^2 + (\sum x_j)^2\right]} \tag{3.17}$$

Now, we must to replace q into Eq. (3.15) to determine c.

$$c = \frac{n\sum x_j r_j \sum x_j + (\sum x_j)^2 \sum r_j}{n^2\left[\sum x_j^2 + (\sum x_j)^2\right]} - \frac{\sum r_j}{n} \tag{3.18}$$

Savitzky-Golay smoothing filter constructs the signal curvature with weighting factor stated by unweighted linear least-squares regression and third order of polynomial. Thus, the best-fit equation ε contains of factors (q_{best}, c_{best}) and based on least squares, regression is utilized to produce the weighting factor W_i .

3.6.1.2 Estimation of Span Level

In order to calculate the Span level of Savitzky-Golay smoothing, we conduct experimentations on numbers of MR images. This method offers the flexibility to carefully obtain the desired Span level through the Savitzky-Golay smoothing filter. Desired Span level of the smoothing filter is achieved based on the gradient of peak point to the next adjacent point of the ACF of noisy image, whilst for greater gradient the desired Span level is at minimum range (near to 0.1) and vice versa. We use the outcomes of these experiments to fit the data and develop a general expression via curve fitting to find the desired Span level for different MR images. Smallest Span level provides a smoothest fit that works well for high Noise variance (NV). Since the curve has characterized by noise, large Span level results in the loss of information data points in different ACF of MR images [39]. We utilized a third degree polynomial curve fitting

to find an expression for Span level evaluation. The expression is displayed in Eq. (3.19).

Linear model polynomial with order of three:

$$f(x) = p_1 x^3 + p_2 x^2 + p_3 x + p_4 , \tag{3.19}$$

Fig. 3.2 evidently displays the gradient of the peak point to next adjacent point of the autocorrelation function along the *x*-axis.

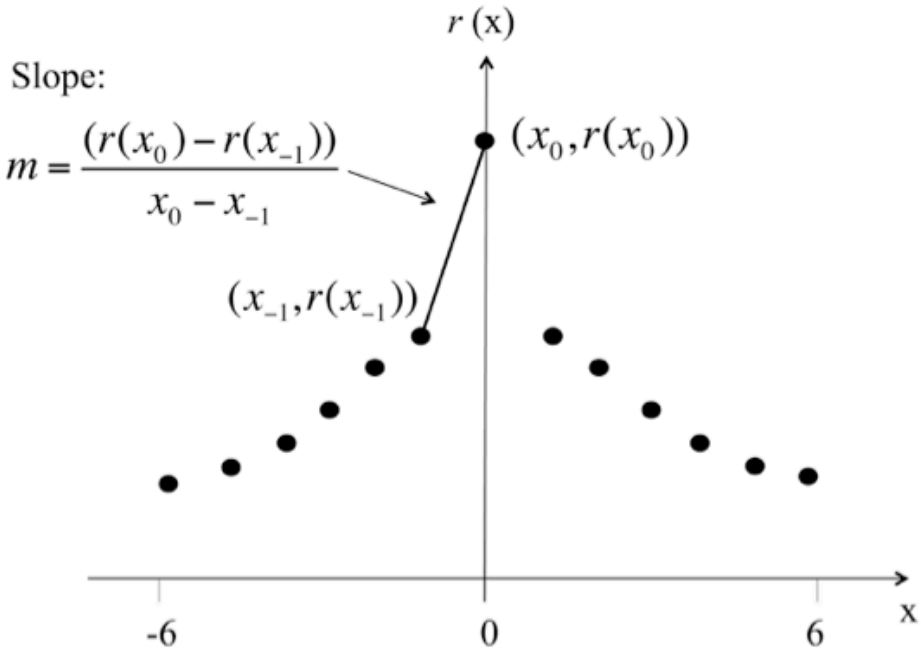

Figure 3.2: Gradient of the ACF peak point to next adjacent point along the *x*-axis [20].

3.6.2 Cross-Correlation SNR estimator using two images

In case of MR images the correlation technique is very valuable technique as they can obtain in the Fourier domain. It is desirable based on processing time to implement a correlation of MR images in the Fourier domain Because of the correlation theorem, which makes the method enormously appropriate for execution in a well-organized way in several MR image acquisition techniques [17]. Subsequently, when the noise is uncorrelated two consequent acquisitions $r_1(\vec{i})$ and $r_2(\vec{i})$ can be utilized to obtain the

SNR [17].

$$r_1(\vec{i}) = s(\vec{i}) + n_1(\vec{i})$$
$$r_2(\vec{i}) = s(\vec{i}) + n_2(\vec{i}) \tag{3.20}$$

The auto-correlation function (ACF) is equivalent to CCF of the two images. Thus, the cross-correlation coefficient (CCC) will be used as displayed in Eq. (3.21).

$$\rho(\vec{i}) = \frac{r_1(\vec{i}) \otimes r_2(\vec{i}) - \langle r_1 \rangle \langle r_2 \rangle}{\sigma_1 \sigma_2} \tag{3.21}$$

While σ_1, σ_2, $\langle r_1 \rangle$ and $\langle r_2 \rangle$ are accordingly the standard deviation and mean of MR image r_1 and r_2.

Chapter 4

PROPOSED SOLUTION

4.1 Introduction

This chapter deliberates the solution to the problem classified in chapter 3; the mathematical proof and the steps to the solution are discussed in details.

4.2 Solution Statement

4.2.1 Single Image Cross-Correlation technique

In order to quantify and improve the SNR using single image, we present a method based on mean and standard deviation of a single image only. We assume MR image r consist of an original signal s corrupted by noise n with zero mean value [17]. Therefore, the system point spread function can be demonstrated as Eq. 4.1.

$$r(\vec{i}) = s(\vec{i}) + n(\vec{i}) \tag{4.1}$$

Where $\vec{i}$ signifies the MR image point. The ratio of the signal standard deviation to the noise standard deviation is displayed in Eq. 4.2.

$$SNR = \sqrt{\frac{\sigma_s^2}{\sigma_n^2}} \tag{4.2}$$

Since the noise is uncorrelated two consequent acquisitions $r_1(\vec{i})$ and $r_2'(\vec{i})$ can be utilized to obtain the SNR [17].

$$\begin{aligned} r_1(\vec{i}) &= s(\vec{i}) + n_1(\vec{i}) \\ r_2'(\vec{i}) &= s(\vec{i}) + n_2'(\vec{i}) \end{aligned} \tag{4.3}$$

We generate r_2' according to r_1 by shifting the n_1 array in a circular manner along one dimension as exposed in section 4.2.3.1 in this thesis. However, the cross-correlation function (CCF) of two images can be calculated as Eq. (4.8)

$$r_1 \otimes r_2' = s \otimes s + n_1 \otimes s + s \otimes n_2' + n_1 \otimes n_2' \tag{4.4}$$

And because the uncorrelated noise, then

$$n_1 \otimes s = s \otimes n_2' = n_1 \otimes n_2' = 0 \tag{4.5}$$

$$r_1 \otimes r_2' = s \otimes s \tag{4.6}$$

We estimate the SNR from the maximum of CCC, and this maximum arises in the center of CCC as displayed in Eq. (4.7), Where $\langle r_1 \rangle, \langle r_2' \rangle$ and $\langle r_1 r_2' \rangle$ are accordingly the mean of MR images r_1, r_2 and both images [17].

$$\rho_m = \frac{\langle r_1 r_2' \rangle - \langle r_1 \rangle \langle r_2' \rangle}{\sqrt{\left[\langle r_1^2 \rangle - \langle r_1 \rangle^2\right]\left[\langle r_2'^2 \rangle - \langle r_2' \rangle^2\right]}} \tag{4.7}$$

4.2.1.1 Noise Level Shifting

In order to generate r_2' we shift the row or column values of n_1 array in a circular manner along one dimension to design a new n_2' matric for different MR images. For example, we shift the n_1 row along vertical dimension by $M/2$ places to obtain n_2', as indicated in Eq. (4.8).

$$n_1(i,j) = \begin{bmatrix} n(1,1) & . & . & n(1,N) \\ . & . & . & . \\ . & . & . & . \\ n(M,1) & . & . & (M \times N) \end{bmatrix}_{M \times N} \Rightarrow n_2'(i,j) = \begin{bmatrix} n(1+(M/2),1) & . & . & n(1+(M/2),N) \\ . & . & . & . \\ . & . & . & . \\ n(M-(M/2),1) & . & . & (M-(M/2),N) \end{bmatrix}_{M \times N}$$

(4.8)

Likewise, In Eq. (4.9) we shift the n_1 column along horizontal dimension by $N/2$ places to obtain n_2'.

$$n_1(i,j)=\begin{bmatrix} n(1,1) & . & . & n(1,N) \\ . & . & . & . \\ . & . & . & . \\ n(M,1) & . & . & n(M,N) \end{bmatrix}_{M\times N} \Rightarrow n_2'(i,j)=\begin{bmatrix} n(1,1+(N/2)) & . & . & n(1,N-(N/2)) \\ . & . & . & . \\ . & . & . & . \\ n(M,1+(N/2)) & . & . & (M,N-(N/2)) \end{bmatrix}_{M\times N} \quad (4.9)$$

Then noisy image $r_2'(\vec{i})$ is generated conforming to Eq. (4.10).

$$r_2'(\vec{i}) = s(\vec{i}) + n_2'(\vec{i}) \quad (4.10)$$

We run experimentations on different type of sample images. We use outcomes of these tests to develop a general expression through curve fitting to determine the preferred n_2' array for different images. We obtain noise level shifting based on three important aspects of an MR image such as, frequency, phase relative to the RF (Radio Frequency) transmitter phase, and magnitude or amplitude as it is shown in Fig. 4.1. We utilized a third degree polynomial curve fitting to attain an expression to obtain the perfect n_2' array for different images. Linear model polynomial with order of three is displayed in Eq. (4.11).

$$f(s) = q_1x^3 + q_2x^2 + q_3x + q_4, \quad (4.11)$$

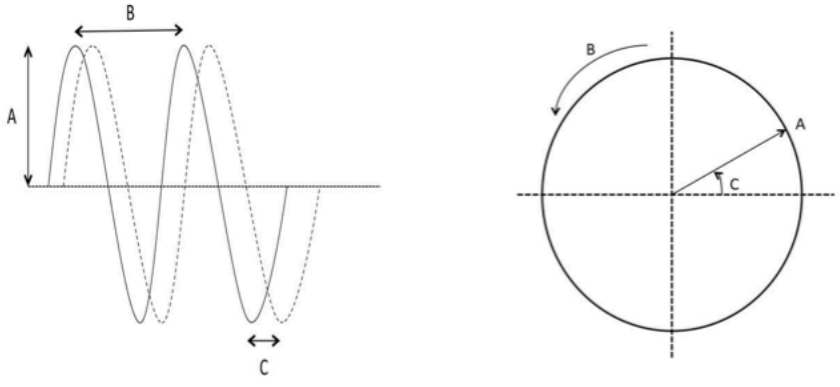

Figure 4.1. Planar and circular demonstrations of time-varying curvature.

In Fig. 4.1 the period (B) is the time needed for accomplishment of one full cycle of the curvature. The amplitude (A) is the maximum derivation of the curvature from its mean

value. The phase angel of curvature (C) elucidates the shifts in the curvature relative original signal. The two plane curvatures demonstrated have the similar period and amplitude, but have a different phase. There are numerous MR signals at some different frequencies following the RF pulse due to existence of many magnets in the magnetic fields.

Eq. (4.12) evidently shows the effect of amplitude, frequency and phase on curvature function.

$$f(t) = A\sin(Bt + C) \tag{4.12}$$

In Eq. (4.12) t is a variable, and other quantities influence the shape of the function. Two of parameters, amplitude A and B remain the same, but phase C changes according to desired noise level shifting. Indeed, we change the function $A\sin(Bt + C)$ across the $t - axis$ by setting $\sin(Bt + C)$ equal to 0, and then we will have Eq. (4.13).

$$(Bt + C) = 0 \tag{4.13}$$

And t is given by Eq. (4.14).

$$t = -\frac{C}{B} \tag{4.14}$$

We simply shift the position of curvature position on the $t - axis$, the shape of the curvature does not change.

The signals are overlaid so that the free induction decay (FID) comprises lots of frequencies fluctuating as a function of time [19]. It is simpler to test multicomponent signal according to frequency rather than of time [19]. The transformation of the signal amplitudes from a function of time to a function of frequency is done by Fourier transformation. The RF pulses as a function of time know FID as response of the net magnetization [19]. Therefore, based on phase relative to the RF transmitter phase,

frequency, and amplitude, we developed a procedure to generate second image using first image in order to quantify SNR estimation. Algorithm I, illustrates the sequence of calculation for the proposed technique.

Algorithm I: Sequence of calculation

1) READ MR image-A
1) ADD Rice noise onto MR image-A
2) APPLY the shift array circularly function onto noisy image (MR image-A) to achieve desired shift to attain MR image-B
3) CALCULATE the mean & standard deviation of MR image-A $\langle r_1 \rangle$
4) CALCULATE the mean & standard deviation of MR image-B $\langle r_2' \rangle$
5) CALCULATE the mean & standard deviation of both MR images $\langle r_1 r_2' \rangle$
6) CALCULATE the mean & standard deviation of squared MR image-A $\langle r_1^2 \rangle$
7) CALCULATE the mean & standard deviation of squared MR image-B $\langle r_2'^2 \rangle$
8) SET calculated values into $\rho_m = \dfrac{\langle r_1 r_2' \rangle - \langle r_1 \rangle \langle r_2' \rangle}{\sqrt{\left[\langle r_1^2 \rangle - \langle r_1 \rangle^2\right]\left[\langle r_2'^2 \rangle - \langle r_2' \rangle^2\right]}}$
9) SUBSTITUTE ρ_m, into $SNR = \sqrt{\dfrac{\rho_m}{1-\rho_m}}$

4.2.2 Cubic spline autoregressive-based interpolator with Savitzky-Golay smoothing

In the earlier work the SNR of SEM images was improved by using smoothing function, which is based on least square by fitting a small set of successive data point into a polynomial [35]. The estimated central of the fitted point polynomial curve is considered as a new smoothed data set [20].

It is assumed that there are a group of known points $(x_0, r(x_0)),(x_1, r(x_1)),...,(x_{j-1}, r(x_{j-1})),(x_j, r(x_j)),(x_{j+1}, r(x_{j+1})),...(x_n, r(x_n))$. For every single data point, third order degree polynomial is used to interpolate among all the known data points [36].

In the case of polynomial function with the order of three, the curve will be as $r_j(x) = a_4 + a_3 x + a_2 x^2 + a_1 x^3$ while the curve passes within all the known points and $r_j(x_j)$ of the coefficients of curvature function can be calculated [36]. Hence, they all can be determined as Eq. (4.15):

$$r_j(x) = \sum_{j=1}^{n+1} a_j x^{n+1-i} \tag{4.15}$$

In Eq. (4.15), $r_j(x)$ is signified as ACF of noisy image. Consequently, coefficients approximation of x according to the third order of polynomial can produce the whole curvature. Sim *et al*. (2014) proposed a filter to remove noise using Savitzky-Golay smoothing filter.

Savitzky-Golay smoothing displays that the set of digits $(W_{-n}, W_{-(n-1)},..., W_{(n-1)}, W_n)$ may be expressed as weighting coefficients but according to polynomial degree and desired Span level to perform the smoothing procedure [20]. These digits can be generated as specifically equivalent for fitting the data to a polynomial in order to diminish the error in estimation of SNR [37]. Therefore, the smoothed data point is demonstrated in Eq. (4.16):

$$\bar{r}_j(n) = \frac{\sum_{i=-n}^{n} W_i r_{j+i}}{\sum_{i=-n}^{n} W_i} \tag{4.16}$$

In Eq. (4.16), $\bar{r}_j(n)$ signifies a third order of polynomial of smoothed data points that is produced by cubic spline interpolation, and W_i is the weighting factor in smoothing the window [20]. To calculate the span level of Savitzky-Golay smoothing, we utilized a third degree polynomial curve fitting to find an expression for Span level approximation [20]. The expression is indicated in Eq. (4.17).

Linear model polynomial with order of three:

$$f(x) = p_1 x^3 + p_2 x^2 + p_3 x + p_4 , \tag{4.17}$$

Savitzky-Golay smoothing filter forms the signal curvature with weighting factor specified by third order of polynomial and unweighted linear least-squares regression [20]. In this thesis, we developed the proposed approach by merging CSISG method with GMMD technique at next section.

4.2.3 Gaussian Mixture Model Decomposition

With respect to the importance of SNR measurements in image analysis especially in MR imaging and the difficulties faced in its measurements, we propose infinite mixture of GMMD for more precise estimation of SNR for different MR images, which depends on the nature of selected MR image such as, high curvature points, sharp edges and extremities of periodic pattern [22]. We conduct experiments on T1 and T2 weighted MRI. This approach provides the flexibility to attain the desired numbers of Gaussian mixtures. In the case of three Gaussian mixtures, the highest peak of Gaussian mixture is called the global maximum whereas two point of local maxima. The global maximum has a major impact on estimation of SNR compare to other two existing sub-optimal set of Gaussian mixtures for different noisy MR images. Therefore, we simply estimate the SNR using CSISG technique for each fitted Gaussian mixture [20], then multiply each estimated SNR by its mixing proportion and sum them up to achieve the final SNR as it is illuminated in Eq. (4.18)

$$SNR_{Sum} = \sum_{i=1}^{k} \pi_i SNR_i \tag{4.18}$$

In Eq. (4.18), k depends on the selected number of Gaussian mixture model components. Figures 4.2 - 4.5 evidently Display five sets of experimental outcomes for four groups of fitted mixture models, which prove the compactness and the accuracy of estimation as the number of GMM increases.

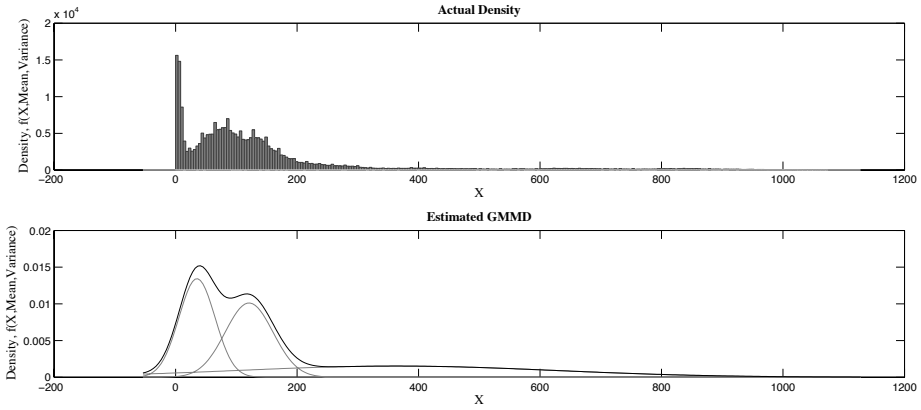

Figure 4.2: Comparison among actual density and the generated Gaussian mixture distribution with 3 components in 1 dimension for *T2-w* spine sample image D as shown in Fig 5.10 (d).

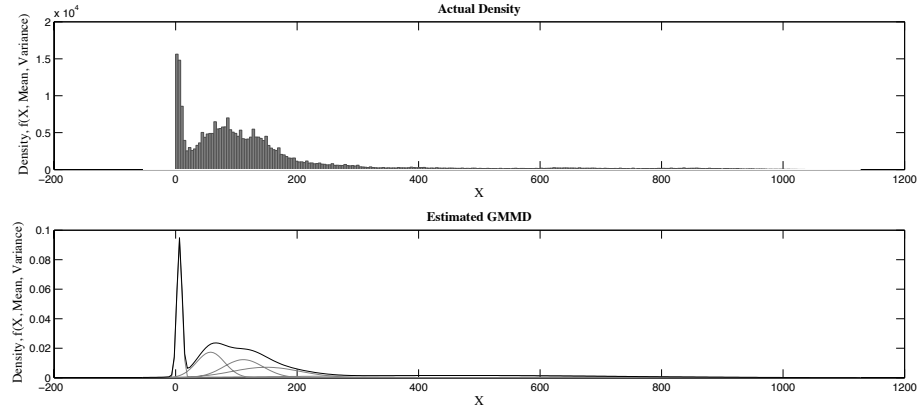

Figure 4.3: Comparison among actual density and the generated Gaussian mixture distribution with 5 components in 1 dimension for *T2-w* spine sample image D as shown in Fig 5.10 (d).

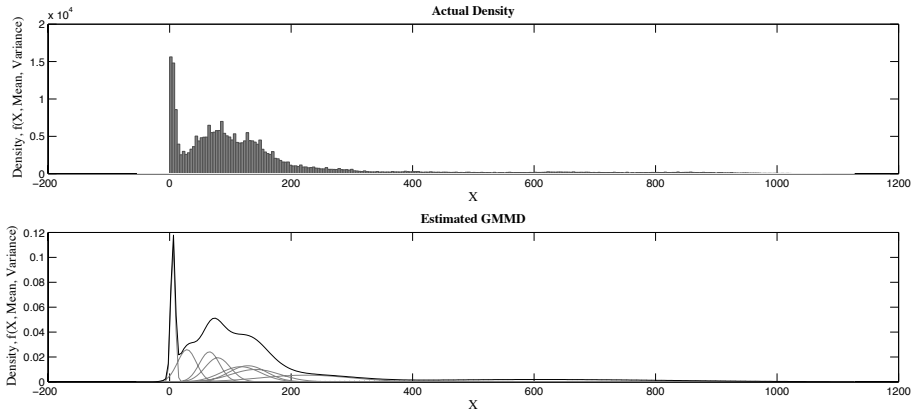

Figure 4.4: Comparison among actual density and the generated Gaussian mixture distribution with 9 components in 1 dimension for *T2-w* spine sample image D as shown in Fig 5.10 (d).

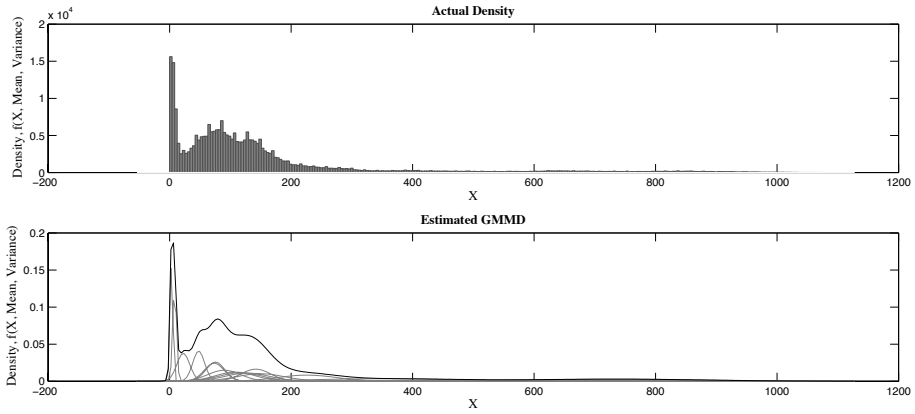

Figure 4.5: Comparison among actual density and the generated Gaussian mixture distribution with 15 components in 1 dimension for *T2-w* spine sample image D as shown in Fig 5.10 (d).

One of the great aspects of GMM is its capability to form smooth approximations to arbitrary formed densities, due to its ability of indicating large class of model distribution. In this thesis, GMMD technique was used to organize the mixed proportion into Gaussian mixture modeling. And the method was successfully applied on MR sample image decomposition in order to evaluate SNR estimation. Algorithm II, illustrates the sequence of calculation for the proposed technique.

Algorithm I: Sequence of calculation

1) READ MR image
2) ADD Rice noise onto MR image
3) GENERATE Gaussian mixture model of MR noisy image
4) CALCULATE the mean value (μ^2) of each generated Gaussian mixture
5) FIND the Noisy ACF peak point $\boldsymbol{r(0)}$ from Gaussian mixture model decomposition (GMMD) of MR image
6) APPLY CSISG filtering onto noisy GMMD of MRI to obtain noise-free (NF) $\overline{r}(0)$ for GMMD
7) SUBSTITUTE achieved point $\overline{r}(0)$ into $SNR = \left(\overline{r}(0) - \mu^2\right) \Big/ \left(r(0) - \overline{r}(0)\right)$

Chapter 5

RESULTS AND DISCUSSIONS

5.1 Introduction

To illustrate the robustness and precision of proposed techniques, we select different MR sample images (DICOM). For each sample image, achieved experimental values are tabulated as SNR, and SNR graphs are also illustrated in this section.

5.2 Image cross-correlation using a single MR Image

In order to express the correctness of proposed method on MR images, we select two sets of *T1-w* MR sample images with $448 \times 448 \times 448$ pixels and *T2-w* MR sample images with $512 \times 512 \times 512$ pixels MR sample images as demonstrated in Fig. 5.1 – 5.2, respectively. We demonstrated the Signal, Noise and SNR separately to display the effect of attracted noise by T1 and T2 weighted MRI using the proposed approach.

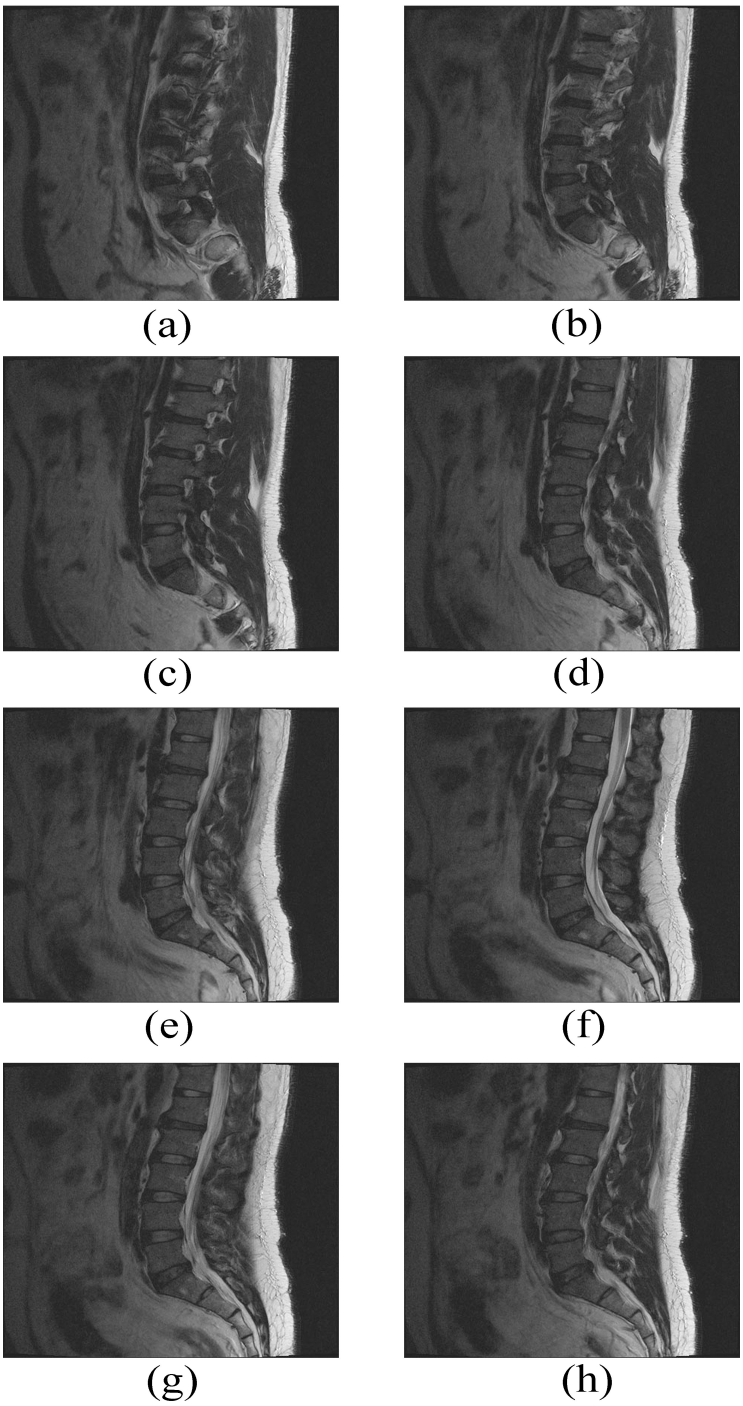

Figure 5.1: *T1-w* MR sample images; (a) spine sample image A; (b) spine sample image B; (c) spine sample image C; (d) spine sample image D; (e) spine sample image E; (f) spine sample image F (g) spine sample image G (h) spine sample image H

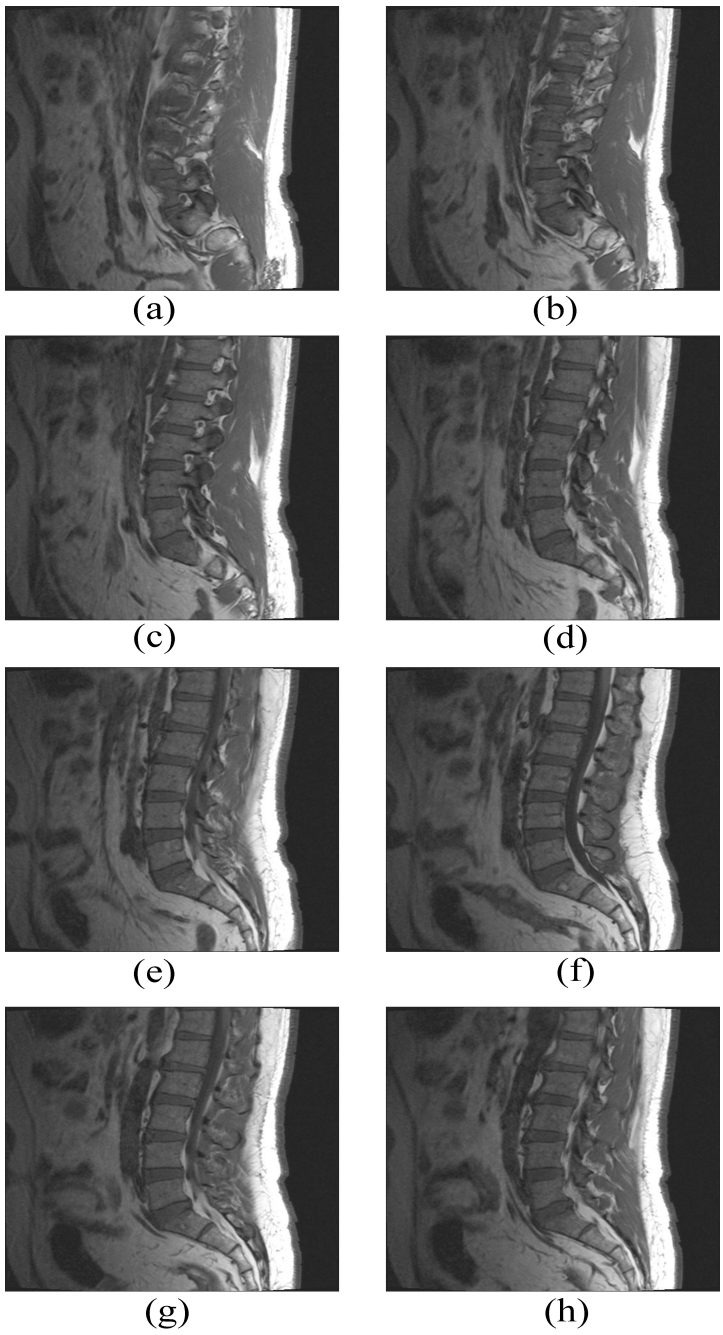

Figure 5.2: *T2-w* MR sample images; (a) spine sample image A; (b) spine sample image B; (c) spine sample image C; (d) spine sample image D; (e) spine sample image E; (f) spine sample image F (g) spine sample image G (h) spine sample image H

Table 5.1: The SNR of spine sample images taken at *T1-w,* as it is shown in Figure 5.1

T1 mode Images	Signal	Noise	SNR
Spine image A	0.3902	1.9947e-06	442.3054
Spine image B	0.3895	2.1870e-06	422.0206
Spine image C	0.3894	3.0674e-06	356.3297
Spine image D	0.3916	9.3336e-06	204.8483
Spine image E	0.3952	6.1267e-06	253.9955
Spine image F	0.3949	5.5937e-06	265.7279
Spine image G	0.3930	5.3931e-06	269.9733
Spine image H	0.3922	6.0978e-06	253.6395

Table 5.1 illustrates the SNR value for T1-Weighted MR images; at lower NV we observe the high SNR and higher NV results to the low SNR.

Table 5.2: The SNR of spine sample images taken at *T2-w,* as it is shown in Figure 5.2

T1 mode Images	Signal	Noise	SNR
Spine image A	0.4770	1.5794e-05	173.7962
Spine image B	0.4703	2.3072e-05	142.7767
Spine image C	0.4694	1.9316e-05	155.8940
Spine image D	0.4711	2.2623e-05	144.3086
Spine image E	0.4718	2.8175e-05	129.4113
Spine image F	0.4695	1.5760e-05	172.5985
Spine image G	0.4721	3.7643e-05	111.9900
Spine image H	0.4691	3.7124e-05	112.4204

Tables 5.1 – 5.2 indicate that the SNR values of T1 relaxation time are higher while compared with T2 relaxation time in all the cases, since T1 relaxation time sample images contain more noise while T2 relaxation time sample images contain lesser noise. Fig. 5.1 shows the good quality of image with fewer numbers of noises, which captured by T1 relaxation time mode.

For more illustration purposes, in order to illustrate the robustness and precision of proposed technique compare to the existing methods, we select different MR sample images with a size of 512×512 pixels as displayed in Fig. 5.3. For each sample image, achieved experimental values are tabulated as SNR, and SNR graphs are also illustrated in this section.

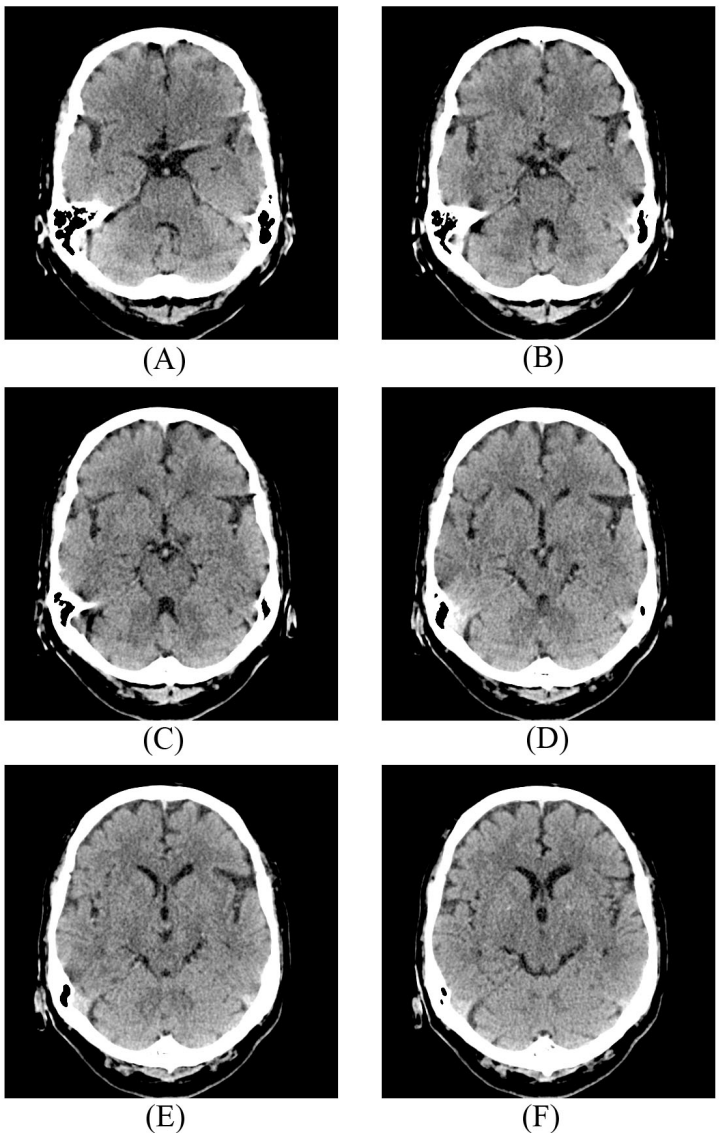

Figure 5.3: 512×512 pixels MR sample images; (A) brain sample image A; (B) brain sample image B; (C) brain sample image C; (D) brain sample image D; (E) brain sample image E; (F) brain sample image F

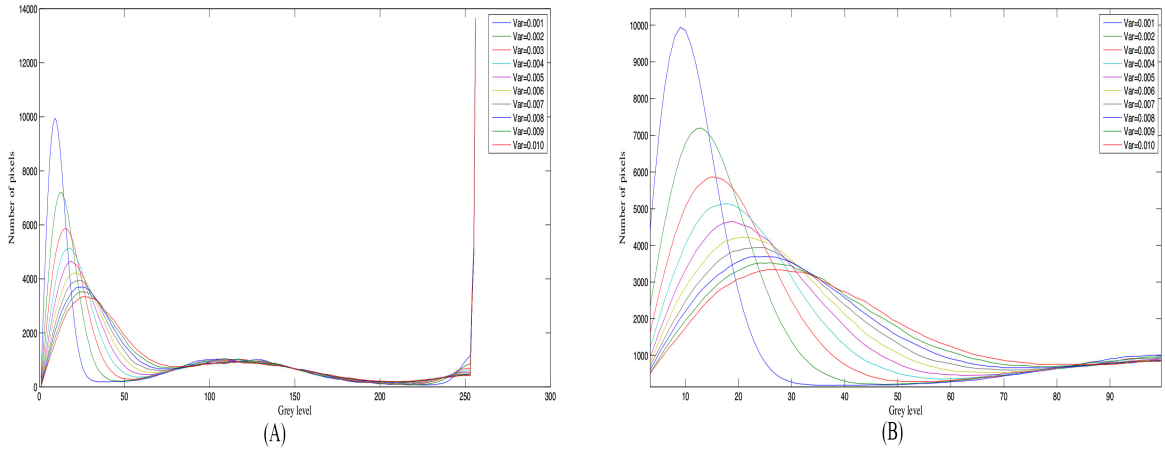

Figure 5.4: (A) Rayleigh curve noise variance of brain sample image A from 0 to 0.010; (B) enlargement of brain image A (left)

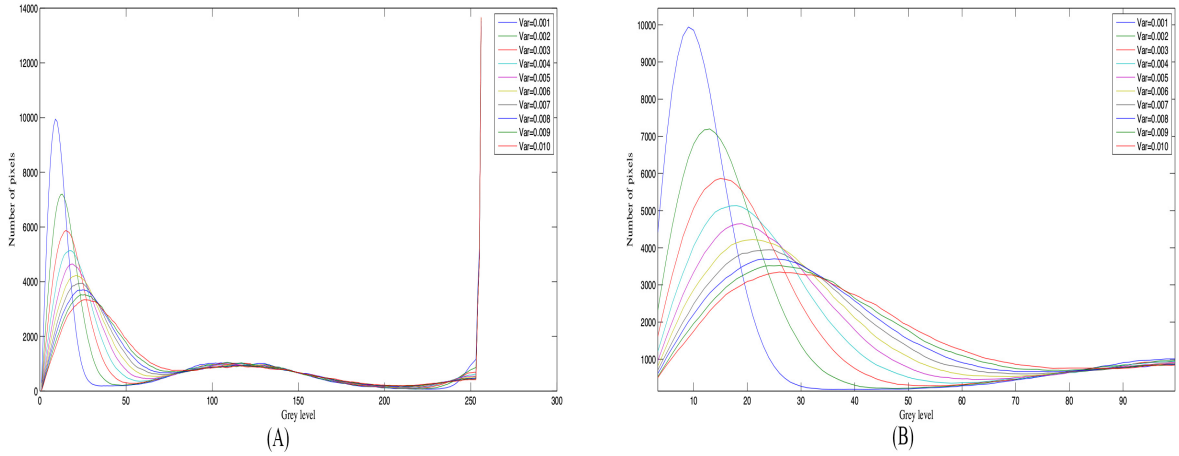

Figure 5.5: (A) Rayleigh curve noise variance of brain sample image B from 0 to 0.010; (B) enlargement of brain image B (left)

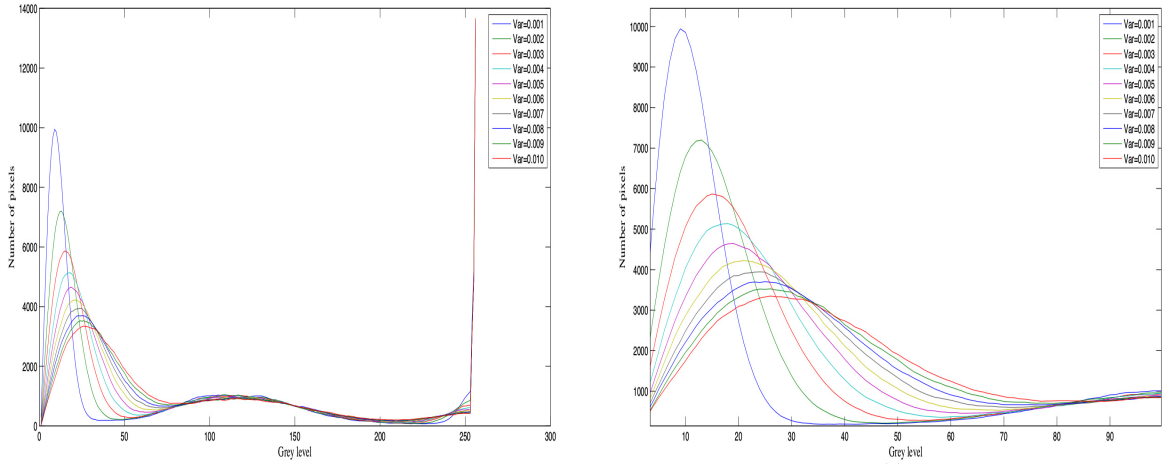

Figure 5.6: (A) Rayleigh curve noise variance of brain sample image C from 0 to 0.010; (B) enlargement of brain image C (left)

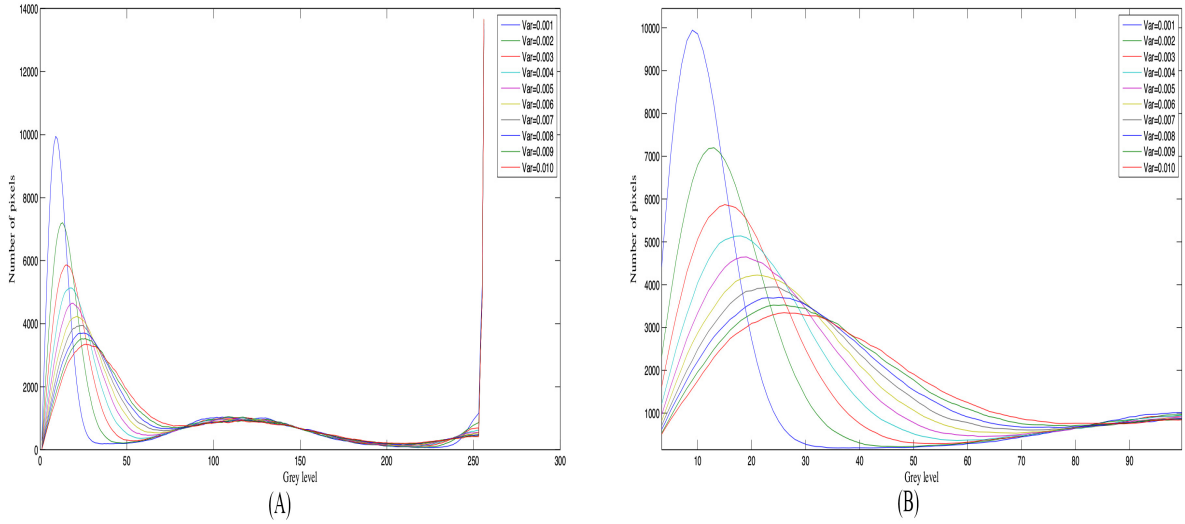

Figure 5.7: (A) Rayleigh curve noise variance of brain sample image D from 0 to 0.010; (B) enlargement of brain image D (left)

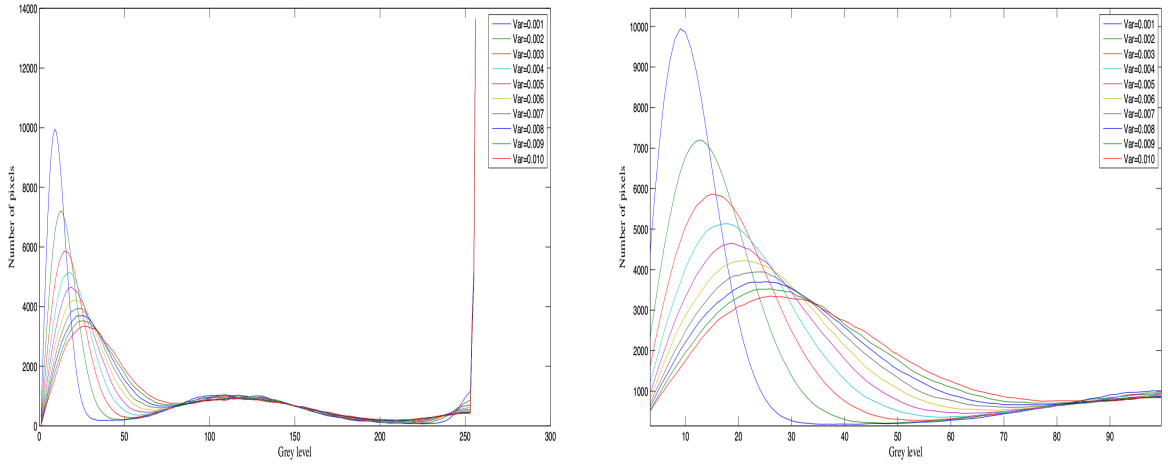

Figure 5.8: (A) Rayleigh curve noise variance of brain sample image E from 0 to 0.010; (B) enlargement of brain image E (left)

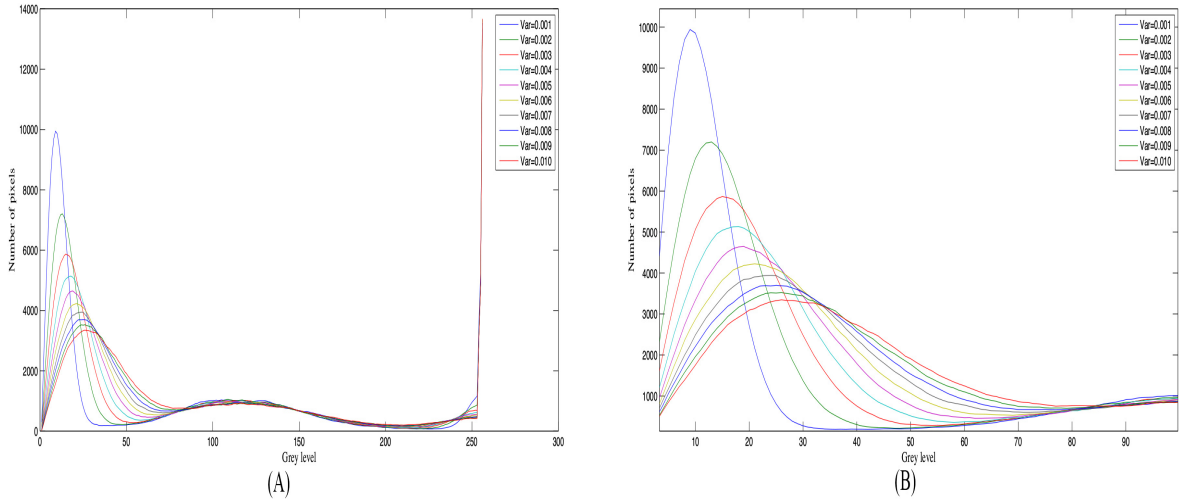

Figure 5.9: (A) Rayleigh curve noise variance of brain sample image F from 0 to 0.010; (B) enlargement of brain image F (left)

Table 5.3: SNR for brain sample image A as it is shown in Fig 5.3(A)

Noise Level or NV	Actual SNR in dB	TIM SNR [30] in dB	SIM SNR in dB
0.1%	26.2313	25.8610	25.9913
0.2%	24.8459	23.1169	22.8162
0.3%	24.1813	23.2878	23.6074
0.4%	23.2718	22.6840	21.8411
0.5%	23.0596	22.5830	22.1390
0.6%	22.6473	22.2600	22.4313
0.7%	22.4949	22.0610	21.7788
0.8%	22.1250	22.2946	22.3228
0.9%	21.9715	22.2613	21.7848
1.0%	21.7933	21.9679	21.6990

From Table 5.3, it can be seen that SIM technique works well for brain sample image a compare to TIM, especially where the NV ranges from 0.003 to 0.010.

Table 5.4: SNR for brain sample image B as it is shown in Fig 5.3(B)

Noise Level or NV	Actual SNR in dB	TIM SNR [30] in dB	SIM SNR in dB
0.1%	25.9984	23.9334	24.8324
0.2%	24.6888	23.4541	23.3723
0.3%	23.9419	22.6721	22.3204
0.4%	23.4664	22.7269	22.1530
0.5%	22.9743	22.6226	22.4557
0.6%	22.6194	23.0719	21.0665
0.7%	22.3861	23.1361	23.1978
0.8%	22.2086	22.1519	21.7619
0.9%	21.9522	21.9853	21.9702
1.0%	21.6650	22.6229	21.1555

Table 5.4 shows that the SNR values of SIM technique are much nearer to TIM technique, and also work truly well where the NV ranges from 0.006 to 0.010 for brain sample image B.

Table 5.5: SNR for brain sample image C as it is shown in Fig 5.3(C)

Noise Level or NV	Actual SNR in dB	TIM SNR [30] in dB	SIM SNR in dB
0.1%	26.0495	25.1577	24.2085
0.2%	24.5525	22.5377	22.1216
0.3%	23.9170	22.7718	22.8725
0.4%	23.4923	21.8522	21.1248
0.5%	22.9597	22.7611	22.1240
0.6%	22.6630	20.2716	21.6042
0.7%	22.3087	21.8906	21.5967
0.8%	22.1515	21.5113	22.3355
0.9%	21.9116	23.3879	23.9568
1.0%	21.6578	22.2764	21.6365

Table 5.5 manifestly shows that SNR values of SIM technique are significantly nearer to TIM technique for brain sample image C, especially where NV ranges from 0.001 to 0.005. This indicates that the SIM technique is more reliable in its performance.

Table 5.6: SNR for brain sample image D as it is shown in Fig 5.3(D)

Noise Level or NV	Actual SNR in dB	TIM SNR [30] in dB	SIM SNR in dB
0.1%	26.4605	24.1509	24.6074
0.2%	24.8537	22.7349	23.1268
0.3%	24.0864	22.8653	24.2057
0.4%	23.5572	23.0098	21.7597
0.5%	23.1188	22.1083	21.5548
0.6%	22.8232	24.5040	21.5764
0.7%	22.6399	22.1644	22.4893
0.8%	22.2900	23.0541	22.6026
0.9%	22.0713	22.2094	21.2307
1.0%	21.8553	22.1431	21.1512

Table 5.6 clearly shows that SIM technique attains the finest results as close as TIM technique for brain sample image D, especially where NV ranges from 0.07 to 0.010.

Table 5.7: SNR for brain sample image E as it is shown in Fig 5.3(E)

Noise Level or NV	Actual SNR in dB	TIM SNR [30] in dB	SIM SNR in dB
0.1%	26.4068	24.7396	24.0868
0.2%	24.9620	23.1019	24.2046
0.3%	24.0525	23.5117	23.9141
0.4%	23.5687	22.9419	21.5793
0.5%	23.3361	22.7396	22.7223
0.6%	22.6623	22.3611	23.1815
0.7%	22.6238	23.0967	22.9954
0.8%	22.5126	23.1877	20.6974
0.9%	22.0804	22.7996	21.7449
1.0%	22.1070	22.2581	22.1160

In the Table 5.7, the SNR values of SIM method are near to TIM technique for brain sample image E, where NV ranges from 0.001 to 0.010.

Table 5.8: SNR for brain sample image F as it is shown in Fig 5.3(F)

Noise Level or NV	Actual SNR in dB	TIM SNR [30] in dB	SIM SNR in dB
0.1%	26.1435	23.9175	23.3957
0.2%	24.8833	23.2985	23.5162
0.3%	24.1317	23.4939	22.0765
0.4%	23.4827	22.5943	22.4822
0.5%	23.0183	22.7686	22.5305
0.6%	22.9904	23.9215	24.3239
0.7%	22.3827	22.6800	21.2481
0.8%	22.1677	22.0843	21.9848
0.9%	21.8293	23.3456	21.8575
1.0%	21.8713	23.4545	22.2323

In the Table 5.8, it is evident that SNR values of SIM estimator are superior for brain sample image F as compared with other exiting method, where especially NV ranges from 0.001 to 0.008.

To test the robustness of SIM technique, we selected the six samples of MR images with different exaggerations as displayed in Fig. 5.3, then CCFs and CCCs are respectively estimated based on different levels of added NVs onto the single sample MR images. The computed SNR values of lower NVs are greater while compared to higher NVs.

Therefore, the accuracy of the SIM technique can be realized from the Tables 5.3 - 5.8 of results as compered to TIM method where NV ranges from 0.001 to 0.010.

5.3 Gaussian Mixture Modeling Decomposition via CSISG Smoothing

In order to show the accuracy and robustness of GMMD-CSISG, we conduct experiment on T1 and T2 weighted MR images (DICOM). For all images, SNR Table is presented in the result section. Plus we produced T-test in order to display the minor difference between the GMMD-CSISG and actual SNR values. T-test estimates a $100 \times (1-\alpha)\%$ certainty interval for the actual mean of **(original SNR)-(GMMD-CSISG SNR)**. P-value of the T-test illuminated in the range of [0,1], and the minor value of P-value exposed the uncertainty in null hypothesis validation [40]. In order to measure the reliability and accuracy of proposed GMMD-CSISG technique, we conduct the experiment on other existing techniques as well as cross correlation function (CCF) and cubic spline interpolation with Savitzky-Golay (CSISG) smoothing for the MR images. The outcomes of GMMD-CSISG and the other existing estimators are demonstrated in Tables 5.9 -5.12.

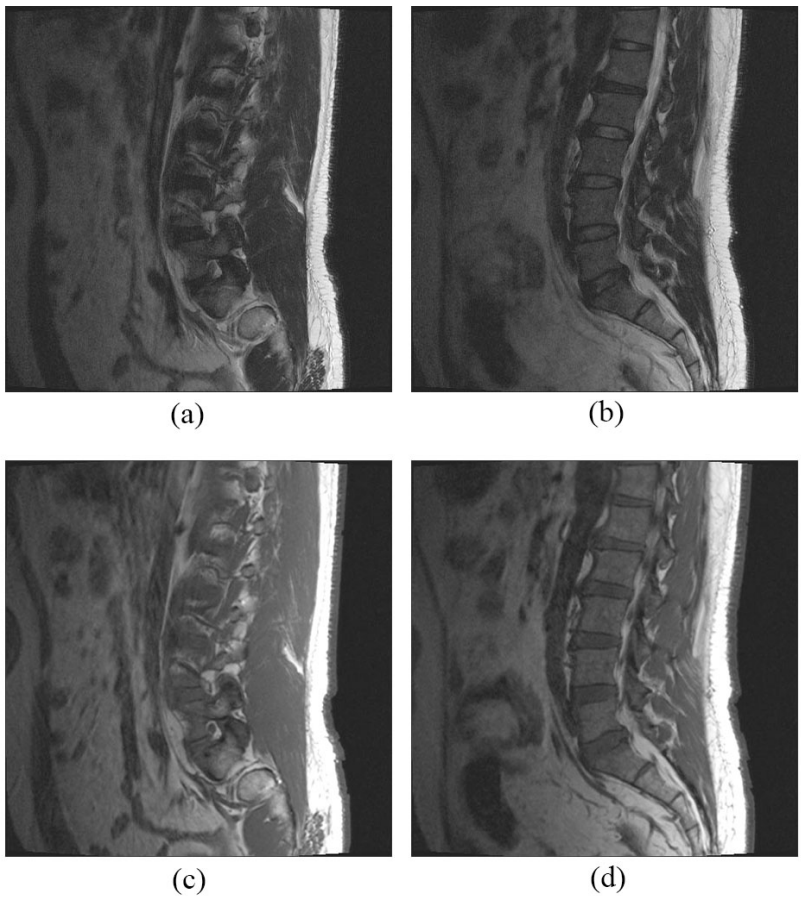

Figure 5.10: 448 × 448 × 448 pixels *T1-w* MR sample images (a) spine sample image A. (b) spine sample image B. 512 × 512 × 512 pixels *T2-w* mode MR sample images (c) spine sample image C. (d) spine sample image D

5.3.1 *T1-w* MRI Data

To show accuracy and effectiveness of GMMD-CSISG method, tests were performed on MRI data with a size of 448 × 448 × 448 T1-w image as displayed in Figures 5.10a - 5.10b. As can be seen from Table 5.9 and Table 5.10, the SNR values of GMMD-CSISG technique is very close to the actual SNR, which shows for different level of noise 3%, 9%, 15% and 21%. Figures 5.11 - 5.12 evidently demonstrates the comparison among results of proposed method and other existing method as well as CCF and CSISG techniques.

Table 5.9: SNR comparison for *T1-w* spine sample image A as shown in Fig 5.10 (a)

Noise level	Actual SNR	Proposed GMMD-CSISG SNR	CCF SNR [30] in dB	CSISG SNR [20] in dB
3%	34.7444	34.1385	31.6986	33.2848
9%	24.5303	24.3977	23.9112	23.8483
15%	19.9572	19.6958	19.2715	19.8778
21%	16.8708	16.5984	19.1837	16.0217

For the sake of clarity, as it is evident in Table 5.9, we have estimated the SNR for *T1-w* MRI. SNR values decline while the level of noise ranges from 3% to 21%. Table 5.1 shows that GMMD-CSISG approach is extremely close to the actual SNR values, while compared to other existing methods. Moreover, *T*-test rejects the null hypothesis at $\alpha = 0.06$ significance level, since *p*-value is equal to 0.0514.

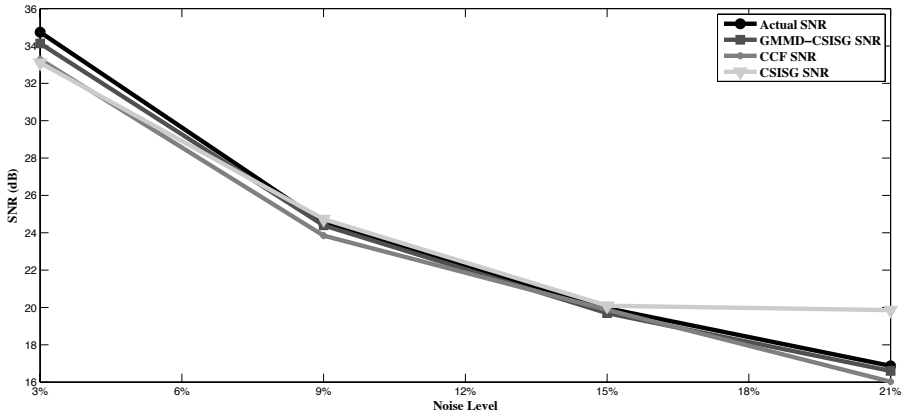

Figure 5.11: Comparison of results of experiment on *T1-w* spine sample image A as shown in Fig 5.3 (b).

Table 5.10: SNR comparison for *T1-w* spine sample image B as shown in Fig 5.10 (b)

Noise level	Actual SNR	Proposed GMMD-CSISG SNR in dB	CCF SNR [30] in dB	CSISG SNR [20] in dB
3%	35.5305	35.3165	31.0802	33.0975
9%	25.2493	25.1132	23.2830	24.7290
15%	20.6631	20.2796	19.9577	20.0894
21%	17.2737	17.0447	19.2718	19.8570

Table 5.10 evidently explains that how SNR values of GMMD-CSISG technique are near to the actual values when compared to CSISG SNR. *T*-test for actual and GMMD-CSISG SNR values indicates the *p*-value of 0.0188 that ignores the null hypothesis at the default $\alpha = 0.05$ level. The *p*-value equal to 0.0188 clarifies that with 95% confidence interval on the mean does not include 0.

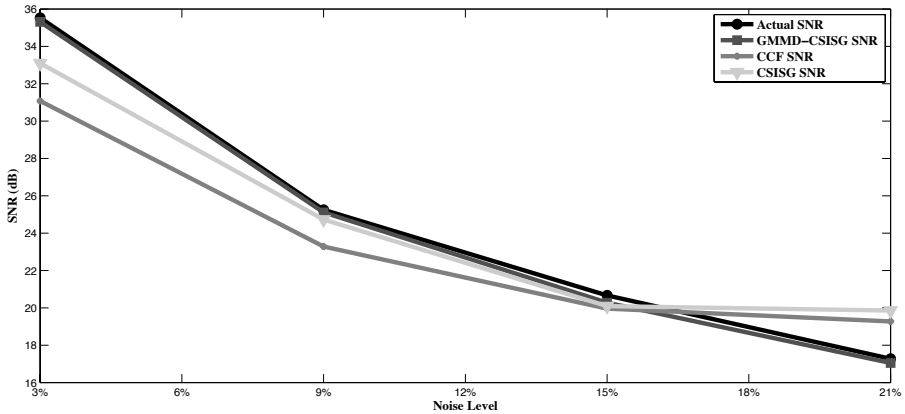

Figure 5.12: Comparison of results of experiment on *T1-w* spine sample image B as shown in Fig 5.10 (b).

5.3.2 *T2-w* MRI Data

For illustration purposes, we used MRI data with size of 512× 512× 512 T2-w image as shown in Figures 5.10c - 5.10d.

Table 5.11: SNR comparison for *T2-w* spine sample image C as shown in Fig 5.10 (c)

Noise level	**Actual SNR**	**Proposed GMMD-CSISG SNR in dB**	**CCF SNR [30] in dB**	**CSISG SNR [20] in dB**
3%	38.4412	38.2824	33.0882	37.4309
9%	28.5578	28.5578	24.1200	25.6447
15%	23.6296	23.3135	22.6504	20.9376
21%	20.7393	20.5964	20.5721	19.7030

Table 5.11 illustrates that GMMD-CSISG SNR values are much closed to the actual SNR values while compared to other existing approaches, while noise level ranges from 3% to 21%. *T*-test rejects the null hypothesis at $\alpha = 0.10$ significance level, since *p*-value is equal to 0.0968.

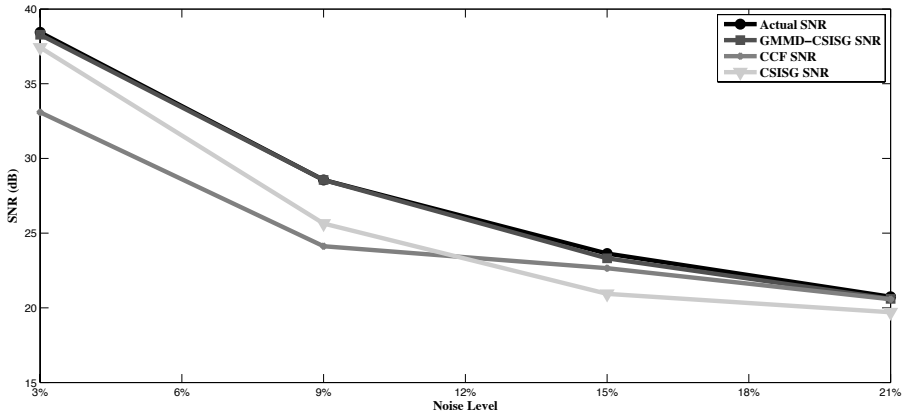

Figure 5.13: Comparison of results of experiment on *T2-w* spine sample image C as shown in Fig 5.10 (c).

Table 5.12: SNR comparison for *T2-w* spine sample image D as shown in Fig 5.10 (d)

Noise level	**Actual SNR**	**Proposed GMMD-CSISG SNR in dB**	**CCF SNR [30] in dB**	**CSISG SNR [20] in dB**
3%	38.3988	38.2444	34.2256	35.2379
9%	27.7305	27.1289	25.5741	26.1636
15%	23.7108	23.6922	22.5904	20.0794
21%	20.3798	20.1751	20.1494	19.4420

In Table 5.12, it is evident that GMMD-CSISG SNR values are significantly closer to the actual SNR values while compared to other existing methods, especially at higher noise level. *T*-test rejects the null hypothesis at $\alpha = 0.15$ significance level, since *p*-value is equal to 0.1456.

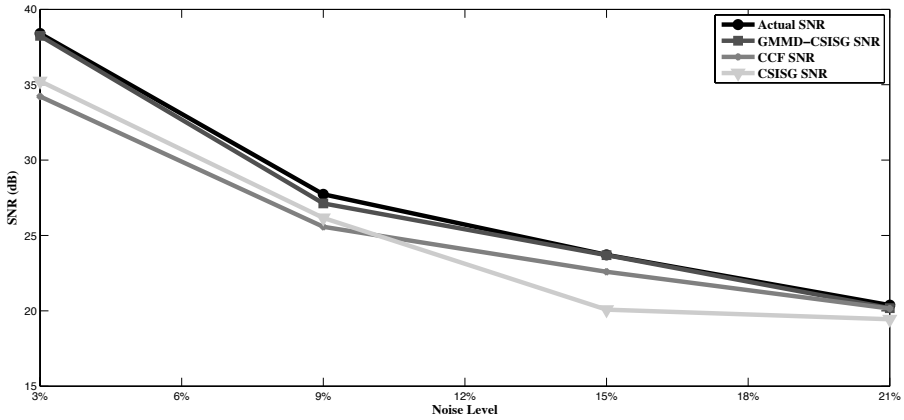

Figure 5.14: Comparison of results of experiment on *T1-w* spine sample image D as shown in Fig 5.10 (d).

Chapter 6

CONCLUSION

6.1 Conclusions

In this thesis, two new approaches of SNR calculation for MRI system is developed and implemented in order to minimize the error. The proposed method applies the CSISG technique in addition to using GMMD algorithm to eliminate the energy of noise and increase the accuracy in SNR estimation. This approach is found to accomplish stunning results while compared with cross correlation function (CCF) and cubic spline interpolation with Savitzky-Golay (CSISG) approaches. Unlike other, the suggested approach is based on a single MR image, which generates consistency and accuracy in SNR estimation. A new noise reduction approach, based on cubic spline interpolation with Savitzky-Golay (CSISG) and GMMD, is developed. The GMMD-CSISG represented the tremendous outcome for SNR evaluation of MR imaging systems.

Another technique has been designed in order to estimate the SNR for MR images. This technique exposed that cross-correlation of two acquisition of the same image could be applied in an extremely efficient approach for the MR system. Images with edge, high curvature and periodic pattern extremities are used in this paper. We conduct several experiments on different MR images according to the important characteristics of an MR image such as, phase relative to the RF transmitter phase, frequency, and magnitude. A general expression for estimation of perfect noise level shifting has been derived using a third degree polynomial curve fitting based on results of these experiments. The procedure uses single MR image to attain SNR value. The capability

to define the SNR from a single MR image allows suggested method to be applicable to online and offline image evaluation instantaneously. The SIM method demonstrated a good presentation for SNR approximation while compared to other existing procedures.

6.2 Future Work

6.2.1 Offline and Online Image Analysis

The proposed methods are applicable to online and offline image investigation for SNR estimation from a single image, where the obligation of image registration with the traditional two-image methods is prohibited.

6.2.2 Real Time Systems

The proposed methods based on a single SNR estimation for MR imaging systems. This feature, in addition to its robustness and accuracy to the power of the accompanied noise, give the technique the conceivability to be applied in real-time procedure for SNR assessment on MR images.

REFERENCES

[1] Sim, K. S., Lai, M. A., Tso, C. P., & Teo, C. C. (2011). Single Image Signal-to-Noise Ratio Estimation for Magnetic Resonance Images. *J Med Syst*. 35, 39-48.

[2] Boone, J. M. (2007). Radiological interpretation, toward quantitative image assessment. *Med Phys*. 34, 4173–4179.

[3] Dietrich, O., Raya, J. G., Reeder, S. B., Ingrisch, M., Reiser, M. F., & Schoenberg, S. O. (2008). Influence of multi-channel combination, parallel imaging, and other reconstruction techniques on MRI noise characteristics. *Magn Reson Imaging*. 26, 754–762.

[4] Wieczorek, H., & Goedicke, A. (2006). Analytical model for SPECT detector concepts. *IEEE Trans Nucl Sci*. 53, 1102–1112.

[5] Gravier, E., Yang, Y.Y., & Jin, M. W. (2007). Tomographic reconstruction of dynamic cardiac image sequences. *IEEE Trans. Image Processing*. 16, 932–942.

[6] Prince, J. L., & Links, J. M. (2006). *Medical imaging signals and system*. New Jersey: Pearson Prentice Hall.

[7] Wang, Y., & Lei, T. (1994). Statistical analysis of MR imaging and its applications in image modeling. *Proc IEEE Int Conf Image Proc Neural Networks*. 1, 866–870.

[8] Brooks, J. C. W., Beckmann, C. F., Miller, K. L., Wise, R. G., Porro, C. A., Tracey, I., Jenkinson, & M. (2008). Physiological noise modelling for spinal functional magnetic resonance imaging studies. *Neuroimage*. 39, 680–692.

[9] Sijbers, J., den Dekker, A. J., Raman, E., & Van Dyck, D. (1999). Parameter estimation from magnitude MR images," *Int J Imaging Syst Technol*., vol. 10, pp. 109–114.

[10] Sano, R. M. (1988). Performance standard for clinical magnetic resonance systems. In: Dixon, R. L. (Ed.), MRI: Acceptance Testing and Quality Control—The Role of the Clinical Medical Physicist Medical Physics. Madison. 185–189.

[11] Murphy, B. W., Carson, P. L., Ellis, J. H., Zhang, Y. T., Hyde, R. J., & Chenevert, T. L. (1993). Signal-to-noise measures for magnetic resonance imagers. *Magn Reson Imaging*. 11, 425–428.

[12] Kaufman, L., Kramer, D. M., Crooks, L. E., & Ortendahl, D. A. (1989). Measuring signal-to-noise ratios in MR imaging. *Radiology*. 173, 265–267.

[13] Henkelman, R. M. (1985). Measurement of signal intensities in the presence of noise in MR images. *Med Phys*. 12, 232–233.

[14] Lenz, F. (1971). Electron microscopy in materials science. London: Academic.

[15] Sim, K. S., Nia, M. E., & Tso, C. P. (2011). Image noise cross-correlation for

signal-to-noise ratio estimation in scanning electron microscope images. *Scanning*. 33, 82–93.

[16] Sim, K. S., Nia, M. E., & Tso, C. P. (2012). Noise variance estimation using image noise cross-correlation model on SEM images. *Scanning*. 35, 205-212.

[17] Zhao, Y., Zhuang, S., & Ting, S.J. (1995). Gaussian mixture density modeling of non-Gaussian source for autoregressive process. *IEEE Trans. Signal Processing*. 43, 894-903.

[18] Zhuang, S., Huang, Y., Palaniappan, K., & Zhao, Y. (1996). Gaussian mixture density modeling, decomposition, and applications. *IEEE Trans. Image Process*. 5, 1293-1302.

[19] Wengrzik, J. W., & Timm, J. (2011). Comparing several methods to fit finite mixture models to grouped data by the EM algorithm. *Proceedings of the World Congress on Engineering*. 1, No. 1.

[20] Sim, K. S., Kiani, M. A., Nia, M. E., & Tso, C. P. (2014). Signal-to-noise ratio estimation on SEM images using cubic spline interpolation with Savitzky–Golay smoothing. *Journal of microscopy*. 253, 1-11.

[21] Sim, K. S., & Kamel, N. S. (2004). Image signal-to-noise ratio estimation using the autoregressive model. *Scanning*. 26, 135-139.

[22] Kiani, M. A., Sim, K. S., Nia, M. E., & Tso, C. P. (2015). Signal-to-noise ratio enhancement on SEM images using a cubic spline interpolation with Savitzky–

Golay filters and weighted least squares error. *Journal of microscopy*. *258*, 140-150.

[23] Meer, P., Jolion, J. M., & Rosenfeld, A. (1990). A fast parallel algorithm for blind estimation of noise variance. *Pattern Analysis and Machine Intelligence, IEEE Transactions on*. 12, 216-223.

[24] Canny, J. (1986). A Computational Approach to Edge Detection," *Pattern Analysis and Machine Intelligence, IEEE Transactions on*. PAMI-8, 679-698.

[25] DC, J., YU, K., & JJ, H. (2000). Metrics of resolution and performance for CD-SEMs. *Proc SPIE 3998*. 108–115.

[26] Thong, J. T., Sim, K. S., & Phang, J. C. (2001). Single-image signal-to-noise ratio estimation," *Scanning*. 23, 328-36.

[27] Sim, K. S., & Kamel, N. S. (2004). Image signal-to-noise ratio estimation using the autoregressive model. *scanning.* 26, 135-139.

[28] Sim, K. S., Chuah, H. T., & Zheng, C. (2005). Performance of a mixed Lagrange time delay estimation autoregressive (MLTDEAR) model for single-image signal-to-noise ratio estimation in scanning electron microscopy. *J Microsc*. 219, 1-17.

[29] Peter, H. (2015). *Nuclear magnetic resonance*. Oxford University Press.

[30] Sijbers, J., Scheunders, P., Bonnet, N., Van Dyck, D., & Raman, E. (1996). Quantification and improvement of the signal-to-noise ratio in a magnetic resonance image acquisition procedure. *Magn Reson Imaging*. 14, 1157–1163.

[31] Sijbers, J., den Dekker, A.J., Van Audekerke, J., Verhoye, M., & Van Dyck, D. (1998). Estimation of noise in magnitude MR images. *Magn Reson Imaging*. 16, 87–90.

[32] McLachlan, G. J., Ng, S. K., & Peel, D. (2003). On clustering by mixture models," In *Exploratory Data Analysis in Empirical Research*. Springer Berlin Heidelberg. 141-148.

[33] Mark, A. B., & Richard, C. S. (2003). MRI: Basic principle and applications. New Jersey: John Wiley & sons, Inc.

[34] Frank, J., & Al-Ali, L. (1975). Signal-to-noise ratio of electron micrographs obtained by cross correlation. *Nature*. 256, 376–379.

[35] Habib, J., Sarfraz, M., & Sakai, M. (2005). Rational cubic spline interpolation with shape control. *Computers & Graphics*. 29, 594-605.

[36] Gerald, C., & Wheatley, P. (1994). Applied Numerical Analysis. Addison-Wesley Publishing Company, Boston.

[37] Gorry, P. A. (1990). General least-squares smoothing and differentiation by the convolution (Savitzky-Golay) method. *Analytical Chemistry*. 62, 570-573.

[38] Douglas, C. M., Elizabeth, A. P., & G. Geoffrey Vining. (2012). Introduction to Linear Regression Analysis. John Wiley & sons, Inc., New Jersey.

[39] Costa, L. D. F., & Cesar, R. M. (2009). Shape classification and analysis: theory and pract ice. CRC Press LLC, Boca Raton, Fla.

[40] Ryan, T.P. (2011). *Statistical methods for quality improvement*. John Wiley & Sons.